NASA TECHNICAL MEMORANDUM TM-75275

MEASUREMENT OF THE TURBULENCE INTENSITY BEHIND A TWO-DIMENSIONAL CASCADE AND IN A THREE-STAGE AXIAL BLOWER

R. Kiock

(NASA-TM-75275) MEASUREMENT OF THE TURBULENCE INTENSITY BEHIND A TWO-DIMENSIONAL CASCADE AND IN A THREE-STAGE AXIAL BLOWER (National Aeronautics and Space Administration) 60 p HC A04/MF A01 CSCL 01A G3/02

N78-26104

Unclas 23391

Translation of "Messung des Turbulenzgrades hinter einem ebenen Schaufelgitter sowie in einem dreistufigen Axialgeblaese," Report 68/32, Institute fuer Aerodynamik der DFL, Braunschweig, 1968, 54 pages + 25 FIGS.

NATIONAL AERONAUTICS AND SPACE ADMINISTRATION
WASHINGTON, D.C. 20546 JULY 1978

STANDARD TITLE PAGE

1. Report No. NASA TM-75275	2. Government Accession No.	3. Recipient's Catalog No.
4. Title and Subtitle MEASUREMENT OF THE TURBULENCE INTENSITY BEHIND A TWO-DIMENSIONAL CASCADE AND IN A THREE-STAGE AXIAL BLOWER		5. Report Date July 1978
		6. Performing Organization Code
7. Author(s) R. Kiock		8. Performing Organization Report No.
		10. Work Unit No.
9. Performing Organization Name and Address Leo Kanner Associates Redwood City, California 94063		11. Contract or Grant No.
		13. Type of Report and Period Covered Translation
12. Sponsoring Agency Name and Address National Aeronautics and Space Administration, Washington, D.C. 20546		14. Sponsoring Agency Code

15. Supplementary Notes

Translation of "Messung des Turbulenzgrades hinter einem ebenen Schaufelgitter sowie in einem dreistufigen Axialgeblaese," Report 68/32, Institute fuer Aerodynamik der DFL, Braunschweig, 1968, 54 pages +25 FIGS.

16. Abstract

Turbulence intensity (Tu) measurements were made in two-dimensional and rotating cascades of blades in a low-speed cascade wind tunnel using hot-wire probes as sensors. The local Tu at Re = $1.6 \cdot 10^5$ was determined in the wake zone behind a two-dimensional cascade. Then the values were recomputed for a rotating cascade, giving a mean turbulence intensity of 6.5% at 1/10 chord downstream and 2.9% at one chord. Fans were used for measurements on the rotating cascade. Re was equal to $7 \cdot 10^5$. Frequency analysis was employed to separate the actual Tu of the entry flow from the effects caused by interaction with the rotor blades, showing that the true Tu increased from a few tenths of a percent to 6.6% in the 1st rotor, and from 7.2 to 9.3% in the 2nd rotor. The Tu behind the 3rd rotor was equal to 8.9%.

17. Key Words (Selected by Author(s))		18. Distribution Statement Unclassified-Unlimited	
19. Security Classif. (of this report) Unclassified	20. Security Classif. (of this page) Unclassified	21. No. of Pages	22. Price

NASA-HQ

MEASUREMENT OF THE TURBULENCE INTENSITY BEHIND A TWO-DIMENSIONAL CASCADE AND IN A THREE-STAGE AXIAL BLOWER

R. Kiock

Abstract /1*

Turbulence intensity measurements were made in stationary (two-dimensional) and rotating cascades of blades in the low-speed cascade wind tunnel of the Institute for Aerodynamics of the DFL Braunschweig. The velocities were in the incompressible range. Hot-wire probes were used as sensors.

In the test section of this wind tunnel, the local turbulence intensity at Re = $1.6 \cdot 10^5$ was determined in the wake defect zone behind a two-dimensional compressor cascade of NACA 65-608 sections. Recalculation of the measured values for a rotating cascade gave a mean turbulence intensity of Tu_m = 6.5% at a distance of 1/10 chord downstream, and 2.9% at a distance of one chord.

The wind-tunnel fan was used for measurements on the rotating cascade. It consisted of three sequentially-arranged single-stage axial blowers which ran at a constant speed. The Reynolds number (Re) was equal to $7 \cdot 10^5$. At the measuring stations in the entry flow to the rotors, the turbulence intensity was adulterated by interaction with the rotor blades. It could be shown on the basis of the frequency spectrum that the true turbulence intensity in the first rotor was increased from a few tenths of a percent to 6.6%, and in the second rotor from 7.2% to 9.3%. Behind the third rotor, Tu was equal to 8.9%.

---

* Numbers in the margin indicate pagination in the foreign text.

TABLE OF CONTENTS

1) Introduction

/3

When the flow behavior of a cascade in a wind tunnel is compared with that of a turbomachine, the turbulence of the flow must be taken into account along with the geometric parameters and the dimensionless quantities of Mach number and Reynolds number. Turbulence means that high-frequency fluctuating velocities are superimposed over the mean velocity of the flow. By measuring certain quantities (turbulence intensity, turbulence spectrum, correlation function, characteristic lengths), it is possible to determine these fluctuating velocities.

In a transition flow the mean velocity obtained from the time integral of the instantaneous velocities is spacially constant. Superimposed over this mean velocity are time-varying turbulent fluctuating velocities, whose temporal (linear) mean value is by definition zero. The ratio of the mean-square of the fluctuating velocities to the mean velocity is called the turbulence intensity.

If we consider the exit flow behind the blades of a stationary cascade, we find that the mean velocity in the wake defect zone is no longer constant. Thus the reference value of the turbulence intensity varies with the coordinate in the test plane in the wake. If this cascade is moved across the flow (rotating cascade), the defect zones follow. A fixed hot wire mounted perpendicular to the flow will then measure the mean value of the instantaneous velocities (= mean velocity) resulting from the wake defects and turbulent fluctuations, as well as the mean-square of all velocity differences with respect to this mean velocity. The latter is constant in a peripheral direction, if we consider a circle with its center as the center of rotation.

Only a few results of turbulence measurements in actual turbomachines have been published to date. De Haller [1] reports that the turbulence intensity in a multistage axial flow compressor under normal operating conditions Tu = 3% behind /4
the first stage, and increases to 5-6% by the end of the machine. In the frequency spectrum, the higher frequencies are predominant. A clear maximum is observed at the blade frequency, i.e. the product of rotary speed and blade number. The spectrum broadens significantly only when the surge limit is approached.

Bahr [2] found a turbulence intensity of 3 to 17% at the outlet of a six-stage axial flow compressor. Tu increases with decreasing compressor speed, intake pressure and choking. With a varying Reynolds number $Re = \bar{c} \cdot l_{mrot}/\nu$, Tu was found initially to decrease with increasing Re ($Re \leq 1 \cdot 10^5$), but remained approximately constant at larger Reynolds numbers. However, the Reynolds number formed by the absolute velocity at the measuring station cannot serve as a reference point for comparison with the flow past other cascades, because in the case of rotating compressor cascades the Reynolds number formed by the relative velocity at the rotor inlet is regarded as the characteristic parameter.

The present investigations were undertaken to shed some light on the turbulence conditions at various points in a multistage compressor. Of particular interest is the rise of turbulence intensity in flow through a cascade of rotor blades. It is our object to determine the turbulence intensity and the frequency spectrum as a function of the through-flow.

To obtain a basis for comparison, we attempted to determine the turbulence intensity behind a two-dimensional stationary cascade of compressor blades. We were interested to learn how the fluctuating velocities vary with the mean velocity in the wake defect.

2) List of Symbols /5

2.1 Geometric Quantities

a_o Axial gap

d_m Mean diameter of annular tunnel

e Vertical distance of cascade exit plane from the test plane in the two-dimensional cascade wake

l Chord length of the two-dimensional cascade

l_{mrot} Chord length of a rotor blade at the mean diameter

l_o Axial length of one fan unit

t Blade spacing

x Coordinate in axial direction of fans

x_t Distance of baffle plate from test section

y Coordinate in the test plane in the two-dimensional cascade wake

z_{rot} Number of rotor blades per wheel

z_{stat} Number of stator blades per wheel

α Angle between absolute velocity and peripheral direction

β Angle between relative velocity and peripheral direction

β_b Blade angle of two-dimensional cascade

δ Angle between flow direction and hot-wire axis

2.2 Flow Quantities

a Velocity of sound

$\bar{c}$ Absolute velocity, mean velocity

$\sqrt{\overline{c'^2}}$ Mean-square of fluctuating velocity

D Decibel (logarithmic ratio measure)

E d.c. voltage value /6

$dE/d\bar{c}$	Slope of calibration curve
$\sqrt{\overline{e^2}}$	Effective value of a.c. voltage
f	Frequency
f_b	Blade frequency
Ma	Mach number
n	Rotary speed of fan
Re	Reynolds number
Tu	Turbulence intensity
u_m	Peripheral velocity at mean diameter
V_M	Through-flow volume
$\bar{w}$	Relative velocity, mean velocity
ν	Kinematic viscosity of air
ϑ	Time

3) Experimental Arrangement and Procedure

3.1 Test Rig

All measurements were carried out in a low-speed cascade wind tunnel. The complete design of this tunnel is described in [3] and is diagrammed in Fig. 1. The two-dimensional cascade was investigated in the test section. It consisted of NACA 65-608 type blades. The following cascade parameters were selected: $t/\iota = 1.0$; $\beta_b = 130°$; $\beta_1 = 140°$ (cf. [4] and Fig. 2). We also selected $Re_1 = c_1 \cdot \iota/\nu = 1.6 \cdot 10^5$. The duct-type fans of the cascade tunnel served as the axial-flow compressor. They consisted of three single-stage axial blowers (Fig. 3) arranged sequentially at a distance of 3.5 rotor blade chords from one another and thus formed in effect a multistage axial flow compressor. All fans operated at the same constant rotary speed and drew in atmospheric air. The /7 inlet section was expanded and fitted with a filtering mat to protect the hot wire from dust. The through-flow was regulated by means of a baffle plate mounted in the test section perpendicular to the flow (Fig. 1). By adjusting the axial distance x_t, the desired through-flow through the fans could be achieved. The secondary outlet was closed off and sealed for the experiment.

The blading of a fan at the mid-radius is diagrammed in Fig. 4. It consists of eight rotors and seven stators. All blades are twisted. The three fans are identical in construction, although each was driven separately.

3.2 Measuring Instruments

The turbulence intensity and the turbulence spectrum were determined by means of a DISA 55 A 01 constant-temperature anemometer. Hot-wire probes were used as sensors: type DISA 55 A 22 (7 mm shaft diameter) for the two-dimensional cascade, and type DISA 55 A 25 (3 mm shaft diameter, Fig. 5) for the fans. A d.c. voltmeter and thermocouple meter were built into the anemometer. The voltmeter operates by virtue of its mechanical inertia to indicate the arithmetic mean of the feed voltage of a bridge circuit and thus the mean velocity. The thermocouple meter supplies the effective value of the a.c. voltage component, which, together with the slope of the calibration curve, yields the effective value of the fluctuating velocity (cf. eqn. 1 and 2). Integration is carried out continuously, with an integration time of 10 to 30 seconds.

For measurements in the fans, the probe was introduced radially into the fan. During both calibration and measurement the probe shaft was positioned perpendicular to the mean velocity direction (it being assumed that the radial component of the mean velocity is negligible).

The indicating characteristics of this hot-wire probe were tested in the wind-tunnel test section before the experiment began. The shaft axis was placed first parallel, then perpendicular to the mean velocity direction, although the hot wire was always perpendicular to the mean velocity during measurements. The turbulence intensities were in good agreement in both cases. /8

The flow angle could also be measured by this probe, since the probe is highly sensitive to rotation about its axis relative to the approach flow (Fig. 6). The minimum of the d.c. voltage reading $E_{min} = f(\delta)$ was sought in each case over the range $\delta = -10°$ to $+10°$. Starting from this angle the hot-wire axis was rotated 90° to place it in a position precisely perpendicular to the mean velocity. The effective value $\sqrt{\overline{e^2}}$, which represents a measure of the turbulence intensity, was read in this position. The high- and low-pass filters were not in operation during the measurements.

The frequency spectrum was determined with the arrangement shown in Fig. 5. Since data evaluation requires a substantial investment of time and equipment, the hot-wire signal was first stored on magnetic tape and was analyzed later. This was done with the aid of a one-third octave filter, which breaks down the total signal into frequency bands with a bandwidth of one-third octave. If f_1 is the lower limit of a one-third octave band, its upper limit is given by $f_2 = \sqrt[3]{2}\, f_1$. The measurable frequency range lay between 20 Hz and 20,000 Hz.[1]

3.3 Measuring Procedure

The calibration curve necessary for finding the turbulence intensity was determined in the test section of the low-speed cascade wind tunnel. A Prandtl tube served as the calibration standard. The slope of this calibration curve is independent of the static pressure p and temperature t with regard to accuracy of measurement, as long as the conditions $\Delta p < 600$ mm H_2O and $\Delta t < 20°$ C are satisfied. Both conditions were, in fact, satisfied in these measurements.

The turbulence intensity in the wake of the middle blade was determined along one blade spacing in the two-dimensional cascade. The downstream distance of the test plane in the wake related to the chord length, e/ι, was equal to 0.10, 0.28, 0.50 and 1.00. /9

The fan investigations were carried out with one, two and three fans driven. Since the fan speed could not be varied from the motor, the through-flow was regulated by blocking the airstream at the exit of the test section with a baffle plate. By

1. We were generously assisted in signal acquisition and evaluation by our colleagues at the Jet Propulsion Institute of the DFL Braunschweig, to whom we again express our thanks.

adjusting the position of this plate, three points on the compressor characteristic could be set for any fan speed. Since the velocities in the fans and test section were in the incompressible range, the mass throughput was proportional to the flow-through volume V_t in the test section. They Reynolds number, formed by the rotor chord length at the mid-radius and the relative velocity at the rotor inlet, was equal to:

$$Re_{1,rot} = \frac{\bar{w}_1 \cdot l_{m,rot}}{\nu} = 7 \cdot 10^5.$$

The stator had a Reynolds number of

$$Re_{2,stat} = \frac{\bar{c}_2 \cdot l_{m,stat}}{\nu} = 4.6 \cdot 10^5.$$

The measuring stations for determining the turbulence intensity are shown in Fig. 3. Most lay at the mid-radius at a distance of 40 mm upstream of the rotor, as well as in the entry plane of the stator. The turbulence intensity was also measured at the following stations:

a) at various distances in front of the rotor and behind the stator of the first fan (the last at the midpoint between the wakes of two rotor blades)

b) at a radius nearer the hub, and one nearer the housing

c) in the inlet plane of the first stator at two additional points in a peripheral direction.

The frequency spectrum was plotted only for a few selected points.

4) Evaluation of Measurements

The hot-wire probe basically measures velocity fluctuations in the direction of the mean velocity. Thus,

$$Tu = 100 \sqrt{\overline{c'^2}}/\bar{c} \; [\%] \qquad (1)$$

Since the hot wire is located in a plane r = const (cylinder jacket) during measurements in the fan, any radial component of the mean velocity is also taken into account, while velocity fluctuations parallel to the wire go undetected. In measurements of Tu, a certain error arises at higher turbulence intensities. Thus, if the radial component of the velocity fluctuation is just as large as the component in the direction of the mean velocity, a relative error of $\Delta Tu/Tu$ = 5% occurs at a turbulence intensity of Tu = 10%. If the component is twice as large, we obtain an error of $\Delta Tu/Tu$ = 20%. The turbulence intensity determined with the above probe arrangement exceeds the true value by these amounts. However, the magnitude of this radial component cannot be ascertained with the measuring instruments available.

The connection between the effective value of the a.c. voltage $\sqrt{\overline{e^2}}$, the d.c. voltage E (both read from the anemometer) and the turbulence intensity is given by the following equation:

$$Tu = \frac{\sqrt{\overline{e^2}}}{\frac{dE}{d\bar{c}} \cdot \bar{c}} \cdot 100 \, [\%], \qquad (2)$$

where $\bar{c}$ is the mean velocity at the measuring station, and $dE/d\bar{c}$ is the slope of the calibration curve $E = f(\bar{c})$.

...GINAL PAGE IS
OF POOR QUALITY

The turbulence intensity for the two-dimensional cascade was determined locally, i.e. at various points in the wake test plane within a blade spacing. In the case of the rotor measurements, only an overall turbulence intensity averaged over the periphery for r = const could be determined. The following discussion will show how, starting from the velocity and turbulence-intensity profile of the two-dimensional cascade, data can be recalculated for the case of a rotating cascade. Fig. 7 shows the velocity-time diagram at an arbitrary point y in the wake zone and the velocity-distance diagram at an arbitrary point in time ϑ. From measurements, we know the mean-square fluctuating velocity $\sqrt{\overline{c'^2}} = f_1(y)$ and the mean velocity $\bar{c} = f_2(y)$: /11

$$\sqrt{\overline{c'^2}} = \frac{1}{\vartheta^*} \int_{\vartheta_1}^{\vartheta_1+\vartheta^*} c'^2 \, d\vartheta \tag{3}$$

$$\bar{c} = \frac{1}{\vartheta^*} \int_{\vartheta_1}^{\vartheta_1+\vartheta^*} c \, d\vartheta \tag{4}$$

with ϑ^* as a sufficiently long integration time, so that the condition

$$\overline{c'} = \frac{1}{\vartheta^*} \int_{\vartheta_1}^{\vartheta_1+\vartheta^*} c' \, d\vartheta = 0 \tag{5}$$

is satisfied.

To recalculate the values for the conditions existing at a rotor, the turbulence intensity must no longer be related to the local mean velocity $\bar{c}(y)$, but to the time- and place-averaged velocity $\overline{c_m}$, which is actually measured behind the rotating cascade:

$$\overline{c}_m = \frac{1}{\vartheta^*}\frac{1}{t}\int_{\vartheta_1}^{\vartheta_1+\vartheta^*}\int_0^t c\;dy\;d\vartheta \tag{6}$$

The path of integration is the blade spacing t. According to Fig. 7, the fluctuating velocity related to $\overline{c_m}$ is given by

$$c'_m = c' + (\bar{c} - \overline{c_m}) \tag{7}$$

and

$$c'^2_m = c'^2 + 2c'(\bar{c} - \overline{c_m}) + (\bar{c} - \overline{c_m})^2 \tag{8}$$

The mean-square of these velocity fluctuations is the double integral over time and distance: /12

$$\sqrt{\overline{c'^2_m}} = \left[\frac{1}{\vartheta^*}\frac{1}{t}\int_{\vartheta_1}^{\vartheta_1+\vartheta^*}\int_0^t c'^2_m\;dy\;d\vartheta\right]^{\frac{1}{2}} \tag{9}$$

From (8) and (9) we have

ORIGINAL PAGE IS
OF POOR QUALITY

$$\sqrt{\overline{c'^2_m}} = \left\{\frac{1}{t}\int_0^t \frac{1}{\vartheta^*}\left[\int_{\vartheta_1}^{\vartheta_1+\vartheta^*} c'^2\,d\vartheta + \int_{\vartheta_1}^{\vartheta_1+\vartheta^*} 2\,c'(\bar{c} - \overline{c_m})\,d\vartheta + \int_{\vartheta_1}^{\vartheta_1+\vartheta^*} (\bar{c}-\overline{c_m})^2\,d\vartheta\right]dy\right\}^{1/2} \tag{10}$$

Since the difference ($\bar{c} - \overline{c_m}$) is time-constant, and since according to eqn. (5)

$$\int_{\vartheta_1}^{\vartheta_1+\vartheta^*} c' \, d\vartheta = 0, \tag{11}$$

eqn. (10) is simplified to

$$\sqrt{\overline{c_m'^2}} = \left[\frac{1}{t}\int_0^t \left[\overline{c'^2} + (\bar{c} - \overline{c_m})^2\right] dy\right]^{\frac{1}{2}}. \tag{12}$$

All the quantities in this equation are known from eqn. (3), (4) and (6), and the turbulence intensity for a rotating cascade is given by

$$Tu_m = 100 \sqrt{\overline{c_m'^2}} \Big/ \overline{c_m} \quad [\%] \tag{13}$$

These equations are valid for the case where the mean absolute velocity measured behind the rotor is equal to the mean velocity $\overline{c_m}$ of the stationary, two-dimensional cascade.

During frequency analysis the effective value was determined as the one-third octave level and complete level in the form of the logarithmic measure D as a function of frequency. With the reference level D = 0 dB according to $\sqrt{\overline{e^2}} = 10^{-6}$ V, /13

$$D = 20 \log \frac{\sqrt{\overline{e^2}}}{10^{-6}}, \tag{14}$$

with $\sqrt{\overline{e^2}}$ in volts. Since we are dealing here not with amplitude values, but with effective values, the addition of one-third octave band levels must be based on the squares of the effective values (= energy of the a.c. voltage):

$$D = 10 \log \left(\frac{\sqrt{\overline{e^2}}}{10^{-6}} \right)^2 \qquad (15)$$

The addition of all octave levels over the entire frequency range must be equal to the complete level:

$$\sqrt{\sum_i (\overline{e^2})_i} = \sqrt{(\overline{e^2})_{dist}} \qquad (16)$$

This is not always true if the accuracy of the one-third octave level diagram is equal to 0.5 dB. Moreover, the energy contained in a frequency band cannot be determined precisely, because there is no filter with a zero transition time ("box filter," cf. Fig. 8). Real filters have a non-negligible transition time and thus indicate only 50% of the energy or 70% of the effective value. Every filter possesses its own characteristic. Some of the energy of adjacent frequency bands is always let through, a situation which is practically impossible to correct for. These errors cancel out, however, if the characteristics of the filters are similar, and if the energy is distributed somewhat uniformly over the spectrum (noise spectrum).

5) Discussion of Results /14

5.1 Turbulence Intensity Behind a Two-Dimensional Compressor Cascade

Fig. 9 shows the turbulence intensity and velocity in the wake defect behind the middle blade for various distances behind the cascade exit plane. The local velocity $\bar{c}_2$ in the wake defect is made dimensionless with the velocity of the undisturbed flow $\bar{c}_{2undist}$ outside the defect zone. The velocity defect becomes broader and flatter with increased distance from the cascade, though even at a distance of one chord there is as yet no mixing with adjacent defects.

The turbulence intensity shows variations similar to $\bar{c}_2$. At the same distance e/l, however, the turbulence intensity profile is somewhat broader than the velocity defect. This is due to the fact that the fluctuating velocities are also higher outside the blade boundary layer near the wall than in the undisturbed flow. Outside the defect, the turbulence intensity $Tu_{2undist} = 0.35\%$. It is thus only slightly higher than in the entry flow to the cascade, where $Tu_1 = 0.25\%$. This increase is caused solely by the delay of the flow as it traverses the blade lattice (cf. eqn. 1).

If we compare the local values of velocity and turbulence intensity in the defect, we see that the turbulence intensity does not vary as a result of the variations of mean velocity according to eqn. (1). This finding is illustrated in Fig. 10. According to the Figure, the locally determined fluctuating velocity undergoes variations similar to the local turbulence intensity in Fig. 9; the change in mean velocity within the defect zone thus has only a slight effect on Tu(y).

Recalculation of this local turbulence intensity for the case where the cascade is rotating in the form of a circular lattice was undertaken according to eqn. (13) and plotted in Fig. 11 over the relative downstream distance of the test plane e/l. Tu_{2m} falls sharply just behind the cascade, attains a value of 2.9% at one chord length, and levels off increasingly /15 with distance from the cascade. This fall of turbulence intensity with increasing distance from the trailing edge was also found in [3] for flow behind a rod lattice.

5.2 Turbulence Intensity and Frequency Spectrum in the Fans

In these measurements the mean velocity as a reference for turbulence intensity can no longer be obtained at single points in the wake defect of the rotor blades. At an arbitrary fixed measuring station, the anemometer is used to take the mean value of temporal fluctuations in velocity, read from the meter as the d.c. voltage E. This corresponds to an averaged velocity $\overline{c_m}$, which now serves as a reference quantity in determining the turbulence intensity.

5.2.1 Variation of Turbulence Intensity Along the Tunnel Axis

Fig. 12 shows the variation of turbulence intensity in the entry flow to the first rotor. The closer the measuring station to the rotor, the greater the apparent turbulence intensity. At a distance of one chord upstream of the rotor inlet plane (station A), Tu = 0.6 to 0.9% (calming effect of filtering mat at inlet), while Tu = 12 to 17% at the distance of one axial gap. It will be shown with the aid of the frequency spectrum that these high values are attributable to velocity fluctuations resulting from the rotating potential field of the rotor blades and cannot be interpreted as true turbulence.

When all three rotors are driven, the flow conditions in all the fans are roughly equivalent, and the measured turbulence intensity is approximately the same at corresponding measuring stations (I,1 - II,1 - III,1 and I,2 - II,2 - III,2) (Fig. 13).

The low turbulence level of the entry flow to the first rotor is not observed again at points between the fans, since these zones are subject to various combined influences. In principle, significantly higher fluctuating velocities occur in a turbulent boundary layer than in a free stream ([5], p. 525). Because $Re = 7 \cdot 10^5$ (rotor) and $4.6 \cdot 10^5$ (stator) here, the boundary layers on the blade surfaces may be regarded as turbulent. Large fluctuating velocities and turbulence intensities occur in the wakes of these blades, therefore. Since measuring stations I,3 through II,1 were located at the midpoint between the wakes of two stator blades, only fluctuating velocities of the first rotor are measured at station I,3 in the case of an unchoked flow. These velocities decay with increasing distance from the rotor, as confirmed by the fall of turbulence intensity between stations I,2 and I,3. The influence of the stator wakes begins at about I,3, and Tu again increases somewhat -- for unlike the measuring station at the stator inlet, the downstream hot-wire probe no longer indicates values averaged over the periphery for r = const, but instead indicates the local values. Thus, depending on the flow angle, the spread of the wake defects in a peripheral direction has varying effects on the values measured at distance x. The variation of turbulence intensity with distance was shown previously in Fig. 9 for the case of the two-dimensional cascade. /16

Starting at station I,7 (82% of the rotor chord in front of the inlet plane of the second rotor), there is a sharp rise of turbulence intensity resulting from interactions with the second rotor. A similar effect was observed in front of the first rotor, as shown in Fig. 12. This means that the turbulence intensity measured at stations I,1, II,1 and III,1 is attributable only in part to pure turbulence. With greater choking of the flow, the rise of Tu begins in the stator, presumably due to boundary layer separation.

When two fans are driven (Fig. 14) and when one fan is driven (Fig. 15), the variation of turbulence intensity along the tunnel axis remains basically unchanged. Of course the level of Tu is higher than in Fig. 13. At a very small delivery volume the flow through the fans is apparently very unfavorable, for the turbulence intensity increases to Tu = 42%. The variation of Tu in the third fan (Fig. 14) and in the second and third fans (Fig. 15) was drawn with a broken line, because their rotors were passively rotated by the airstream, and the flow conditions there were essentially different from in the driven rotors. /17

5.2.2 Variation of Turbulence Intensity in a Vertical and Peripheral Direction

At several stations the turbulence intensity was measured not just at the mid-radius, but at two additional points on the vertical: at a distance of 20% of the tunnel span from the hub, and 20% from the housing wall. A direct effect of the wall on Tu can be excluded due to the relatively large distance involved.

The variation of turbulence intensity in a vertical direction in front of the first rotor is shown in Fig. 16, and behind the first rotor in Fig. 17. Common to the curves in both Figures is a rise of turbulence intensity from the hub to the housing; in front of the rotor this rise is inversely proportional to the variation of mean velocity. According to eqn. (1) the velocity variations are thus independent of the coordinate in the radial direction. Behind the rotor the vertical distribution of mean velocity is approximately constant. The high turbulence intensities in the outer region of the annular tunnel are presumably due to boundary layer separations at the trailing edges of the rotor blades.

Fig. 10 shows the vertical variation of turbulence intensity behind the first stage. The distance to the stator exit plane is slightly more than one stator chord length. The curves show no uniform tendency, because mixing of the rotor wakes in the vertical direction is nonuniform. This was also observed in flow past a stationary lattice of parallel rods ([6], p. 531).

The distribution of turbulence intensity in a peripheral direction is shown in Fig. 19 for the case of the stator inlet plane of the first fan. The measuring stations lay at a distance of 20% of the stator blade spacing from the pressure side and from the suction side of the adjacent stator blades. The turbulence intensity was found to be practically constant at these stations. This means that the potential field of the stator blades had no influence on turbulence intensity in the region investigated. /18

In Fig. 16 through 19, the upper graph shows the turbulence intensity for an approximately constant through-flow and various numbers of fans. These curves almost coincide, showing that equal through-flows give approximately equal turbulence intensities (constant rotary speed). Large discrepancies are observed only in Fig. 18 in the stator exit flow, which is presumably the result of variations in wake mixing. The lower graphs in these four Figures show the turbulence intensity for an unchoked flow but various through-flows. We observe the same tendency as in Fig. 12-15; the higher the through-flow, the lower the turbulence intensity.

5.2.3 Effect of Through-Flow on Turbulence Intensity

The above-mentioned functional relationship between Tu and V_t is clearly seen in Fig. 20 through 22. One is struck by the strong, almost linear fall of turbulence intensity with increasing through-flow. This holds for measuring stations both in front of and behind a rotor. Following a line V_t = const, we observe two things: First, Tu is higher in front of a rotor than behind it. As stated earlier, this is due to the adulteration of the hot-wire signal by interaction with the rotor blades. Second, the more fans are driven, the higher the turbulence intensity. This is understandable at the measuring stations in the third fan (Fig. 22), since here the flow is disturbed by its passage through the fans upstream. It is unclear, however, why these discrepancies, though slight, also arise in the first and second fans (Fig. 20 and 21).

The largest through-flow corresponds to the unchoked condition, while the fans operate near the surge limit at the smallest V_t. In the latter case the turbulence intensity attains its highest values, since here the boundary layers on the suction side separate from the blade surfaces as the result of unfavorable blade entry flow, producing a wide blade wake. /19

5.2.4 Frequency Spectrum

Fig. 23 and 24 show the frequency spectra recorded at the first and second fans. The logarithmic ratio D, as a measure of the energy of velocity fluctuations (cf. eqn. 15), was plotted over frequency. This plot expresses at least qualitatively the magnitude of the velocity fluctuations per frequency band in relation to the total signal (corresponding to the turbulence intensity shown in Fig. 12-22). The width of the frequency bands in this logarithmic plot is constant. Since the frequency analysis was accomplished with a one-third octave filter, the width of three frequency bands corresponds to a doubling of frequency (= octave).

The spectra in front of the first rotor are shown in the top graphs in Fig. 23 for the maximum and mean through-flow. Since all the energy is contained in a few discrete frequency bands, we are dealing with a line spectrum. The frequencies 400, 800 and 1200 Hz are located at the center of these bands. These values correspond to the blade frequency resulting from the rotary speed (n = 2930 rpm) and rotor blade number (z_{rot} = 8):

$$f_b = z_{rot} \cdot n/60 = 8 \cdot 2930/60 = 391 \text{ Hz}$$

and its integral multiples (= harmonics). This means, therefore, that most of the total signal arises from the periodic velocity variations in the rotor entry flow (rotating potential field), due to interaction with the rotating cascade of blades.

The one-third octave band levels alongside these relative maxima, for instance at f = 320 Hz and 510 Hz, are attributable to the swung sides of the one-third octave filter and so are spurious. In an ideal filter, marked levels would probably be produced only at the blade frequency and its harmonics. The noise component (= turbulence) is very slight in these line spectra. /20

The lower graphs in Fig. 23 show the corresponding spectra behind the first rotor. The character of these spectra is different in that the energy is distributed more uniformly over the frequency range. This is a typical sign of the presence of turbulent fluctuating velocities. Here, too, the blade frequency and its harmonics are predominant in the spectrum, but not to the degree observed in front of the rotor. As was shown earlier in the case of the two-dimensional cascade, the fluctuating velocities of the free flow are strongly increased during flow past the blades. If, as in the present case, the cascade and its attendant wakes are rotated, maxima of the fluctuating velocity follow for the blade frequency and its harmonics. These fluctuating quantities, which as in Fig. 7 are related to the mean velocity in the peripheral direction $\overline{c}_m$, produce a true turbulence.

By comparing the two lower spectra in Fig. 23, we see that the fluctuating velocities increase with increased choking, especially at low and middle frequencies (f < 5000 Hz). This broadening of the spectrum as the surge limit is approached has also been observed by de Haller [1].

The two spectra for the second fan (Fig. 24) differ little from each other. The discrete frequencies are still prominent in front of the rotor, while only a slight difference is present behind the rotor. The values measured in front of the second fan again contain velocity fluctuations resulting from interaction with the rotor blades, which thus exaggerate the /21 fluctuating velocity. These components were ascribed to the peaks extending far above the flat turbulence spectrum (see top graph in Fig. 24). It is shown in the sample calculation in the Appendix how these velocity fluctuations are eliminated from the overall spectrum. We than obtain a true turbulence intensity, based solely on fluctuating velocities, of Tu_{corr} = 7.16%.

The turbulence intensity corrected with the aid of frequency analysis was plotted in Fig. 25 together with the raw data for comparison. In front of the first fan the correction supplied very imprecise results, since a line spectrum with a very small noise component was present there, resulting in a large error due to the non-negligible transition time of the filters. The true turbulence intensity here amounts to a few tenths of a percent, as supplementary studies at a greater distance from the blade leading edge have shown (cf. Fig. 25). The true turbulence intensity rises sharply in the first rotor, and from the exit plane on it is identical to the measured Tu. Shortly before the second rotor, measurements are again adulterated by interaction with the rotor blades. If the curve is extrapolated downstream from the first stator and thus eliminates this interaction, Tu = 7.5% at station II,1. This value is in good agreement with that calculated by correction with the aid of frequency analysis (Tu_{corr} = 7.16%). This also demonstrates that the spectrum has smoothed out considerably from station I,2 behind the first rotor to station II,1 in front of the second rotor, and that the above correction has left no fluctuating velocities unaccounted for. Within the second rotor the true turbulence intensity again increases sharply and behind it agrees with the measured value of Tu.

5.3 On the Comparison of Test Data

It is questionable whether one can compare experimental data obtained in cascades of varying blade and cascade geometry at different Mach and Reynolds numbers. A change in /22 but one of these parameters can have a strong influence on the results. Comparison is useful, however, if one deals in terms of orders of magnitude and tendencies.

Some results of turbulence measurements in compressors under operating conditions close to the design point have been summarized in the table on the next page.

According to the table, the turbulence intensity behind the first rotor is equal to 3-6%. The Tu_m value of 4.3% recalculated for a rotating cascade (from a two-dimensional one) also falls within this range. The lower limit may be less than 3, of course: Bahr found Tu = 3% behind the 6th rotor,

a. Autor	b. Quelle	c. Versuchs-anlage	d. Meßstelle	e. Turbulenzgrad
F.de Haller	[1]	f. vielstufiger Axialverdichter	g. hinter der 1.Stufe	Tu = 3 °/o
			h. hinter den letzten Stufen	Tu = 5 — 6 °/o
J. Bahr	[2]	i. sechsstufiger Axialverdichter	j. hinter dem 6.Laufrad	Tu = 3 — 10 °/o
R. Kiock	k. hier	l. ebenes Verdichter-schaufelgitter	m. e/l = 0,28 wie bei Lüfter	n. umgerechnet auf umlaufendes Gitter Tu_m = 4.3 °/o
R. Kiock	k. hier	o. Lüfter, alle Lauf-räder angetrieben	p. hinter dem 1.Laufrad	Tu = 6.6 °/o
			q. hinter dem 2.Laufrad	Tu = 9.3 °/o
			r. hinter dem 3.Laufrad	Tu = 8.9 °/o

Key:
a. Author
b. Source
c. Test rig
d. Measuring station
e. Turbulence intensity
f. Multistage axial flow compressor
g. Behind 1st stage
h. Behind last stage
i. 6-stage axial flow compressor
j. Behind the 6th rotor
k. here
l. Two-dimensional compressor cascade
m. e/l = 0.28 as at fan
n. Recalculated for rotating cascade, Tu_m = 4.3%
o. Fans, all rotors driven
p. Behind 1st rotor
q. Behind 2nd rotor
r. Behind 3rd rotor

ORIGINAL PAGE IS OF POOR QUALITY

implying that the turbulence intensity, which is known to rise during flow through a multistage machine, is smaller in the first stage. An increase in turbulence with the number of stages was found by de Haller (Tu from 3 to 6%), and in the present work during fan measurements (Tu from 6 to 9%). The latter measurements also showed that this increase occurs primarily from the first to second rotor, and that the turbulence intensity varies only slightly farther downstream.

6. Summary /23

This report presents the results of turbulence intensity measurements in a two-dimensional compressor cascade and in the fans of the low-speed cascade wind tunnel of the Institute for Aerodynamics of DFL Braunschweig. The two-dimensional cascade consisted of NACA 65-608 blades. The measurements were made for an operating point in the optimal working range at distances of 1/10 to 1 chord length behind the cascade. The Reynolds number was equal to $1.6 \cdot 10^5$.

The fan measurements were carried out on three single-stage, sequentially-arranged axial blowers which operated at a constant speed. The through-flow was controlled by blocking the flow in the test section with a baffle plate. Re was equal to $7 \cdot 10^5$. The measuring stations were at a distance of one axial gap in front of and behind each rotor as well as at various distances in front of the first rotor and behind the first stator. A hot-wire probe served as sensor in all cases.

The turbulence intensity profiles measured behind the two-dimensional cascade were slightly broader than the velocity profiles. Like the latter, they became wider and flatter with distance. The local variations in fluctuating velocity were similar to the local turbulence intensity variations; that is, the change in mean velocity within the wake defect had little

influence on turbulence intensity. The turbulence intensity recalculated for a rotating cascade Tu_m was found to equal 4.3% at a distance corresponding to the relative axial gap of a fan ($e/l = 0.28$).

During measurement of the approach flow to a rotor, the potential field accompanying the rotating blades produced marked effects. We found Tu = 15% at a distance of one axial gap in front of the entry plane, and only Tu = 0.8% at a distance of one rotor chord. At a distance of one axial gap behind the first rotor, we found Tu = 6 to 22%. The smaller the through-flow, the higher the turbulence intensity. If we compare the results behind the individual stages at a maximum through-flow, we find that the turbulence intensity increases from Tu = 6.6% behind the first rotor to Tu = 9.3% behind the /24
second rotor and then remains approximately constant (Tu = 8.9% behind the third rotor). These results agree with those of other authors in terms of tendency and order of magnitude.

The frequency spectrum, which slows qualitatively the distribution of the energy of velocity fluctuations over the frequency range, revealed that the flow was low in turbulence in front of the first rotor. The apparent high turbulence intensity at this point was due to velocity fluctuations resulting from interactions with the rotor blades. Behind the rotor the energy was distributed more uniformly over the frequency range (= turbulence). In front of the second rotor, the energy peaks above the flat turbulence spectrum were eliminated by calculation, and a turbulence intensity could be determined based entirely on the fluctuating velocities. This correction supplied the true turbulence intensity, which rose from 7.2 to 9.3% in the second rotor, and from a few tenths of a percent to 6.6% in the first rotor.

7) References

1. de Haller, P., "The behavior of cascades of airfoils in axial flow compressors and in a wind tunnel," VDI-Berichte 3, 27-31 (1955).

2. Bahr, J., "Measurements of turbulence intensity in an axial flow compressor," Report 63/8, Institute for Aerodynamics of DFL Braunschweig, 1963.

3. Kiock, R., "Studies on the effect of turbulence intensity on the laminar-to-turbulent transition and on boundary layer separation on compressor blades," Report 67/14, Institute for Aerodynamics of DFL Braunschweig, 1967.

4. Bahr, J., "Studies on the effect of section thickness on flow through two-dimensional compressor cascades at high subsonic speeds," Part I: "Studies in incompressible flow," Report 60/26, Institute for Aerodynamics of DFL Braunschweig, 1960.

5. Schlichting, H., Grenzschicht-Theorie [Boundary Layer Theory], 5th edition, G. Braun, Karlsruhe, 1965.

6. Corrsin, S., "Turbulence: experimental methods," in: Handbuch der Physik [Handbook of Physics], Vol. VIII/2, Springer-Verlag, Berlin, 1963.

Legends to Figures

Fig. 1: The low-speed cascade wind tunnel of the DFL.

a) 3 Axial blowers
b) Power: 3 x 10.5 kW
c) Throughput: 6.7 to 3.4 m^3/s
d) Compression: 3 x 184 mm H_2O
e) Rotary speed: 2930 rpm
f) Secondary discharge (adjustable)
g) Diffuser
h) Straightener
i) Test section
j) Nozzle
k) Baffle plate
l) Tunnel data:
m) Drive power N = 31.5 kW
n) Throughput V = 6.7 to 3.4 m^3/s
o) Static pressure q_1 = 15 to 250 mm H_2O
p) Velocity U_1 = 15 to 65 m/s
q) Test cross-section:
r) Width b_k = 300 mm
s) Height (variable) h_k = 250 to 500 mm

Fig. 2: Arrangement of the two-dimensional cascade.

Fig. 3: Arrangement of the measuring stations in the fans of the low-speed cascade wind tunnel.

a) Filtering mat
b) Total wind production of the tunnel
c) Fan I
d) Power = 3 x 10.5 kW
e) Throughput = 6.7 to 3.4 m^3/s
f) Compression = 3 x 184 mm H_2O
g) Rotary speed = 2930 rpm
h) LA = rotor
i) LE = stator
j) Fan II
k) Fan III
l) Section A-B
m) Longitudinal section through a fan

Fig. 4: Cross-section through a fan of the low-speed cascade wind tunnel.

Fig. 5: Block diagrams for determining the frequency spectrum.

a) Hot wire (platinum-plated tungsten wire 5 μ in diameter and 1.2 mm long)
b) Hot-wire probe type DISA 55 A 25

[Key continued next page]

c) Storage of hot-wire signal on magnetic tape
d) Hot-wire probe
e) Constant-temperature anemometer DISA 55A01
f) Tektronix 545 A oscilloscope
g) Bruel & Kjaer 2112 linear amplifier
h) AMPEX FR 1300 magnetic tape device, 1.5 m/s
i) Frequency analysis of stored hot-wire signal
j) AMPEX FR 1300 magnetic tape device, 1.5 m/s, 4 m endless loop
k) Bruel & Kjaer 2112 analyzer (one-third octave filter) with auxiliary filter
l) Bruel & Kjaer 2305 level recorder with 50 dB potentiometer

Fig. 6: Angle characteristic of a hot-wire probe.

Fig. 7: Velocities behind a two-dimensional cascade.

a) Velocity-time diagram at an arbitrary point y
b) Velocity-distance diagram at an arbitrary point in time ϑ

Fig. 8: Mode of operation of the ideal and real filter.

a) Ideal filter ("box filter"), 100% energy
b) Real filter, 50% energy
c) Interaction of the filters of adjacent frequency bands

Fig. 9: Local turbulence intensity benind a two-dimensional compressor blade cascade.

Fig. 10: Local fluctuating velocity benind a two-dimensional compressor blade cascade.

Fig. 11: Effect of distance on the turbulence intensity determined from eqn. (13).

Fig. 12: Effect from rotor blades on the entry flow.

a) Fans I, II and III driven
b) Plane of blade tips of the first rotor
c) Axial gap
d) Rotor chord $l_{m,rot}$ = 140 mm

Fig. 13: Turbulence intensity along the tunnel axis with three fans driven.

a) Fans I, II and III driven

Fig. 14: Turbulence intensity along the tunnel axis with two fans driven.

a) Fans I and II driven

Fig. 15: Turbulence intensity along the tunnel axis with one fan driven.

a) Fan I driven

Fig. 16: Variation of turbulence intensity over the height of the tunnel in front of the first rotor.

a) Measuring station I,1
b) Driven fans
c) Unchoked
d) Hub
e) Housing

Fig. 17: Variation of turbulence intensity over the height of the tunnel behind the first rotor.

a) Measuring station I,2
b) Driven fans
c) Unchoked
d) Hub
e) Housing

Fig. 18: Variation of turbulence intensity over the height of the tunnel behind the first stage.

a) Measuring station I,5
b) Driven fans
c) Unchoked
d) Hub
e) Housing

Fig. 19: Variation of turbulence intensity in the stator inlet plane of the first fan.

a) Measuring station I,2
b) Driven fans
c) Unchoked
d) Stator pressure side
e) Stator suction side

Fig. 20: Effect of throughput on the turbulence intensity in the first fan.

a) Number of fans driven
b) Measuring station I,1
c) Measuring station I,2

Fig. 21: Effect of throughput on the turbulence intensity in the second fan.

a) Number of fans driven
b) Measuring station II,1
c) Measuring station II,2

Fig. 22: Effect of throughput on the turbulence intensity in the third fan.

a) Number of fans driven
b) Measuring station III,1
c) Measuring station III,2

Fig. 23: Frequency spectrum in the first fan at various throughputs.

Fig. 24: Frequency spectrum in the second fan.

a) Effect from rotor blades
b) Turbulence

Fig. 25: Measured and corrected turbulence intensity along the tunnel axis.

a) Fans I, II and III driven
b) Tu determined from measurements
c) Estimated variation of the true Tu
d) True Tu corrected with spectrum

Deutsche Forschungsanstalt für Luft- u. Raumfahrt (DFL) Institut für Aerodynamik	APPENDIX Sample calculation for spectrum eval., stat. II,1	Blatt Nr. 28

$$\overline{e^2}\,[V^2] = 10^{-12+D/10}$$ after eqn. (15)

$$Tu\,[\%] = 100\,\frac{\sqrt{\overline{e^2}}}{\frac{dE}{d\bar{c}}\cdot\bar{c}}$$ after eqn. (2)

$$Tu_{corr.}[\%] = \frac{\sqrt{\overline{e^2_{dist}} - \overline{e^2_b}}}{\frac{dE}{d\bar{c}}\cdot c}$$

	f [Hz]	D [dB]	$\overline{e^2}$ [V^2]	$\frac{\overline{e^2_{dist}} - \overline{e^2}}{\overline{e^2_{dist}}}$	$\sqrt{\overline{e^2}}$ [V]	Turbulenzgrad [%]
D_{dist}	20 – 20,000	104.6	0,02880	1.00	0.170	12.03
D_1	400	102.6	0,01820	0,63		
D_2	800	91.9	0.00155	0.05		
D_3	1200	85.6	0.00036	0.01		
			$\overline{e^2_{dist}}$ = 0.02011	0.69	0.142	10.05
D_{11}	400	89.2	0,00083	0.03		
D_{22}	800	86.2	0.00042	0.01		
D_{33}	1200	84.9	0.00031	0.01		
			$\overline{e^2_b}$ = 0,00156	0,05	0,040	2,83
			$\overline{e^2_b} = \overline{e^2_{b+r}} - \overline{e^2_r}$ = 0.01855	0,64	0,136	9.63
			$\overline{e^2_{r,dist}} = \overline{e^2_{dist}} - \overline{e^2_b}$ = 0.01025	0.36	0.101	7.16

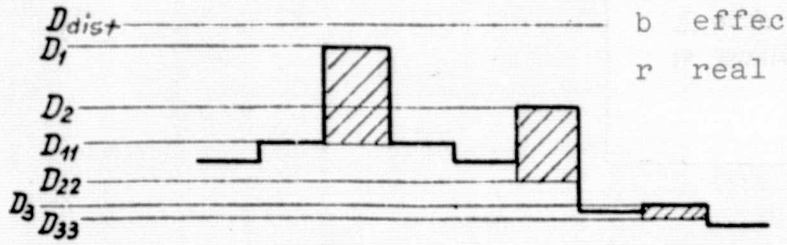

Subscripts

b effect from blades

r real turbulence

Bearbeitet: Klock Franz	Datum: 19.9.68	Skizzenblatt Nr.:	Bericht Nr.: 68/32

Wilh. Fehrig, Braunschweig T 21300

Deutsche Forschungsanstalt für Luft- u. Raumfahrt (DFL) Institut für Aerodynamik	Der Niedergeschwindigkeits-gitterwindkanal (NGK) der DFL	Blatt Nr. 29	Fig. 1

a) *3 Axialgebläse*
b) *Leistung 3 × 10,5 KW*
c) *Durchsatz 6,7 bis 3,4 m^3/s*
d) *Pressung 3 × 184 mm WS*
e) *Drehzahl 2930 U/min*

f) *Nebenablaß (verstellbar)*

g) *Diffusor*

h) *Gleichrichter*

i) *Meßstrecke*

j) *Düse*

k) *Prallplatte*

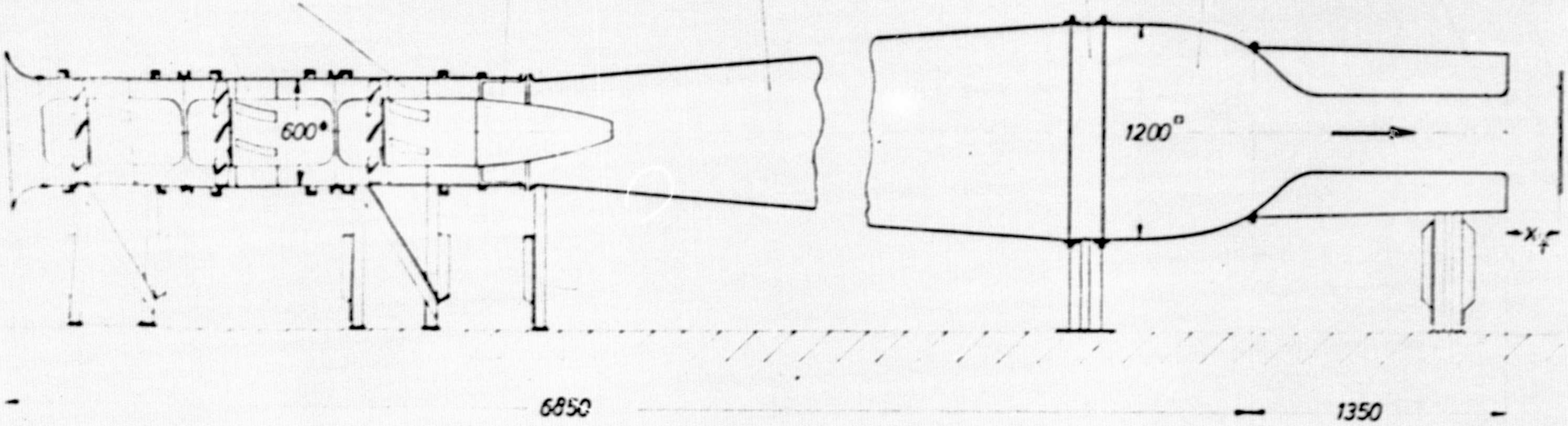

l) **Kanaldaten:**

m) Antriebsleistung	$N = 31{,}5$ KW	q)	Meßquerschnitt:	
n) Durchsatz	$V = 6{,}7$ bis $3{,}4\ m^3/s$	r)	Breite	$b_K = 300$ mm
o) Staudruck	$q_1 = 15$ bis 250 mm WS	s)	Höhe (verstellbar)	$h_K = 250$ bis 500 mm
p) Geschwindigkeit	$U_1 = 15$ bis 65 m/s			

Bearbeitet: Kiock	Datum: 5.4 67	Skizzenblatt Nr.:	Bericht Nr. 68/32

Deutsche Forschungsanstalt für Luft- u. Raumfahrt (DFL) Institut für Aerodynamik	Anordnung des ebenen Gitters	Blatt Nr. 30 / Fig. 2

NACA 65 – 608		
$t/l = 1.0$	$\beta_b = 130°$	$Re_1 = 1.6 \cdot 10^5$
$l = 60mm$	$\beta_1 = 140°$	$Ma_1 = 0.12$
		$Tu_1 = 0.25\,\%$

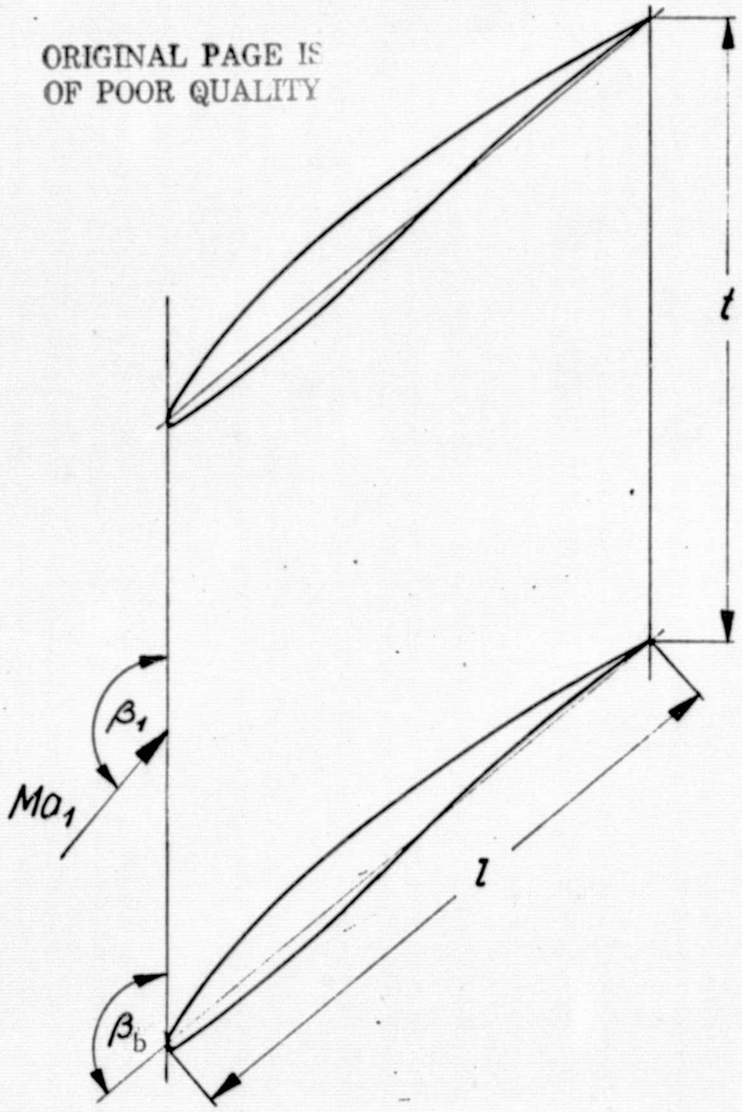

Bearbeitet: Kiock Franz	Datum: 10.9.68	Skizzenblatt Nr.:	Bericht Nr.: 68/32

Wilh. Fahrig, Braunschweig T 21300

Deutsche Forschungsanstalt für Luft- u. Raumfahrt (DFL)
Institut für Aerodynamik

Anordnung der Meßstellen an den Lüftern des NGK

Blatt Nr. 31

Fig. 3

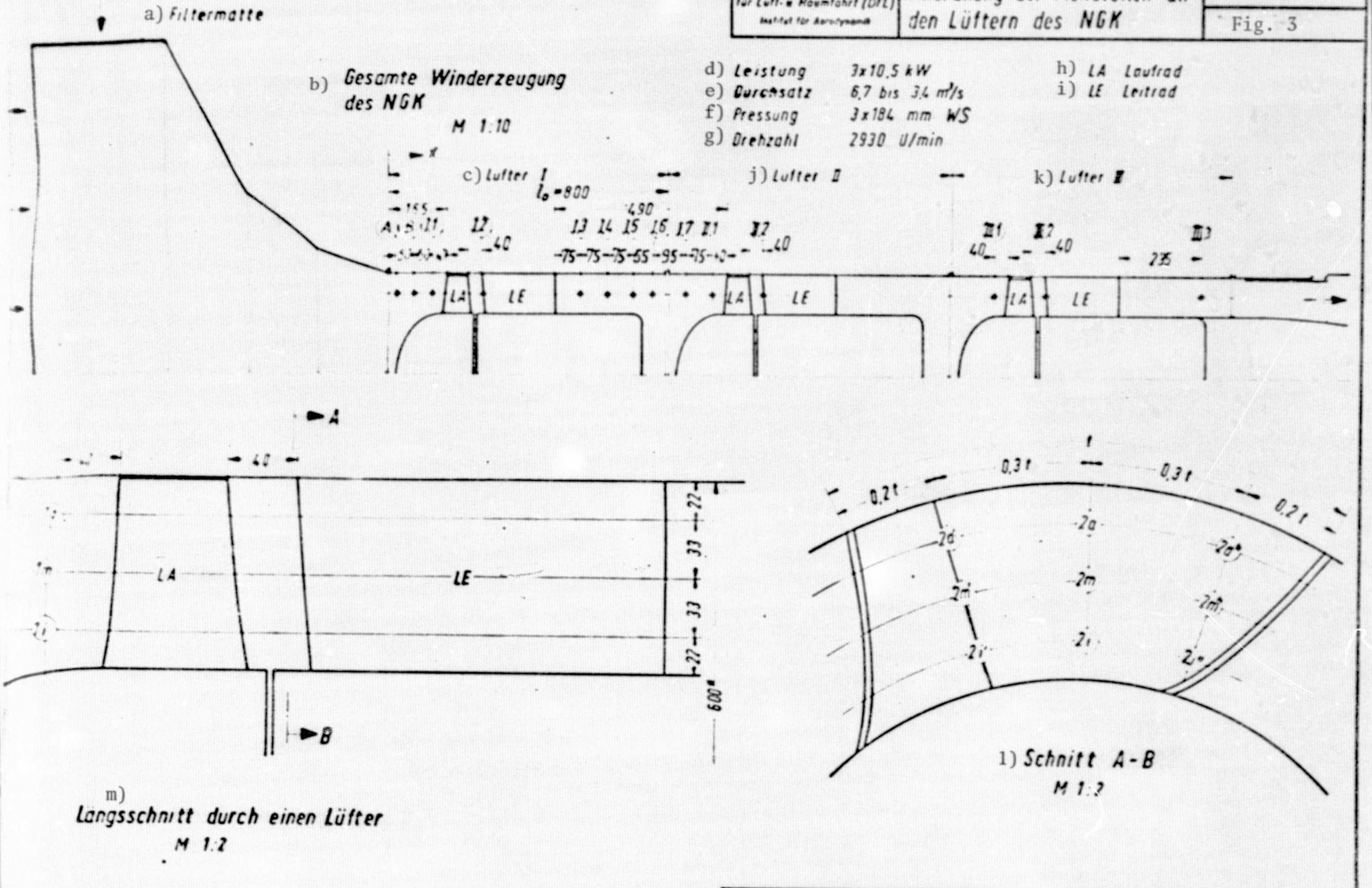

Bearbeiter: Kiock / Rath

Datum: 8.4.1968

Skizzenblatt Nr.:

Bericht Nr. 68/32

Deutsche Forschungsanstalt für Luft- u. Raumfahrt (DFL) Institut für Aerodynamik	Mittelschnitt durch einen Lüfter des NGK	Blatt Nr. 32
		Fig. 4

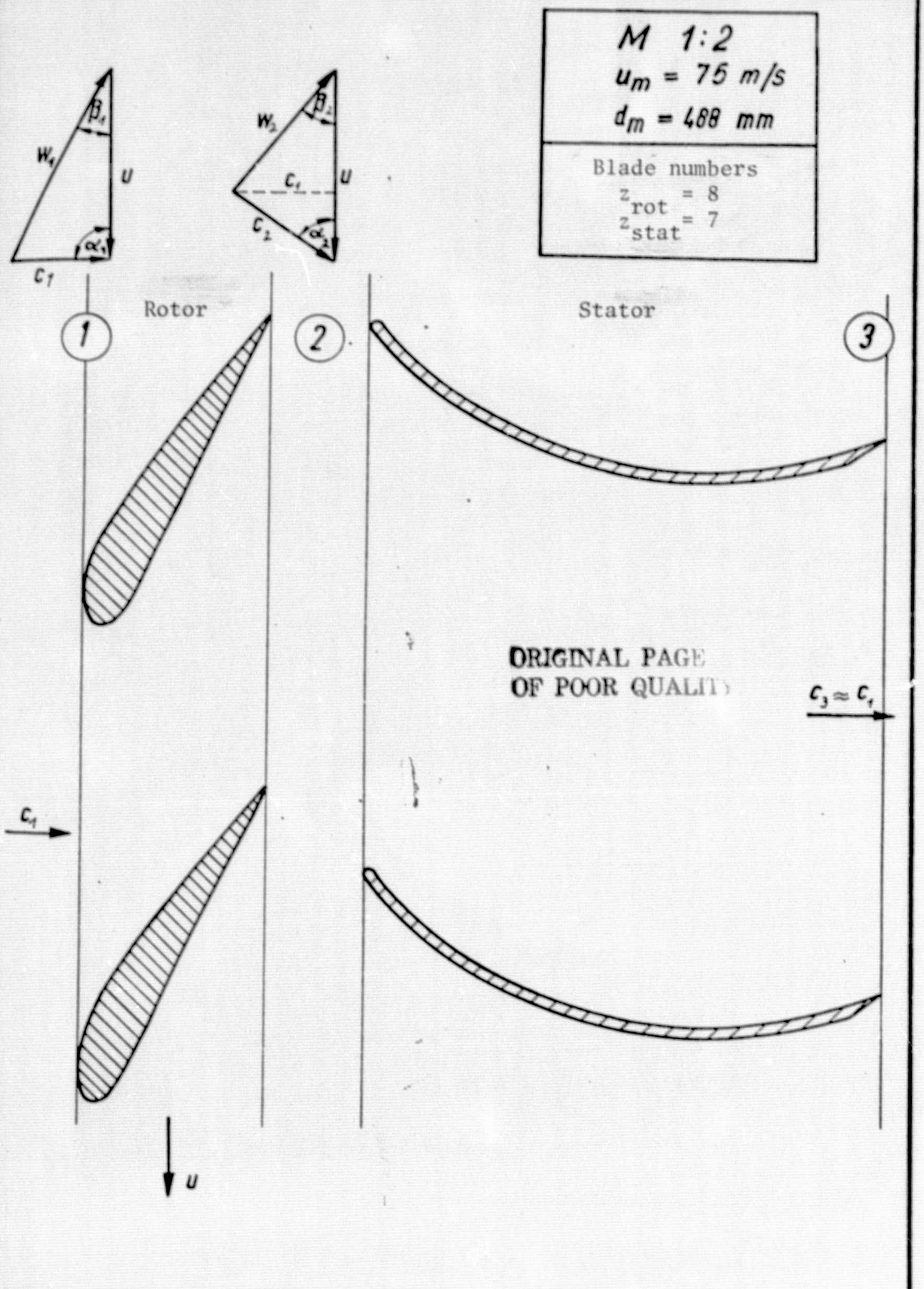

Bearbeitet:	Datum:	Skizzenblatt Nr.:	Bericht Nr.:
Kiock – Janiak	25.4.68		68/32

Wilh. Fehrig, Braunschweig T 21300

Deutsche Forschungsanstalt für Luft- u. Raumfahrt (DFL) Institut für Aerodynamik	Blockschaltbilder zur Ermittlung des Frequenzspektrums	Blatt Nr. 33
		Fig. 5
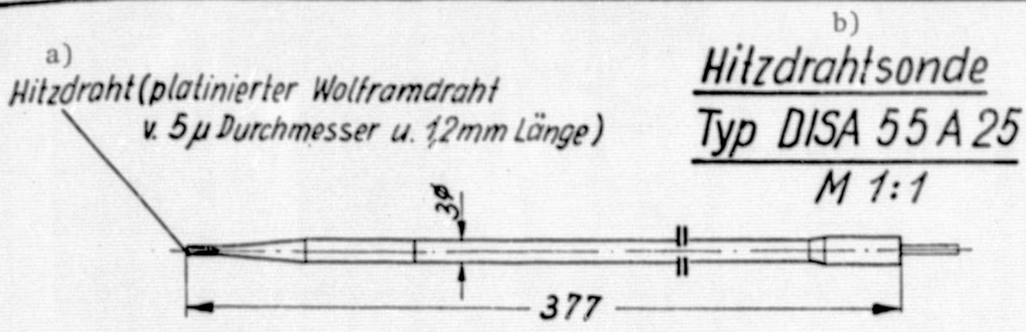
c) Speicherung des Hitzdrahtsignals auf Magnetband

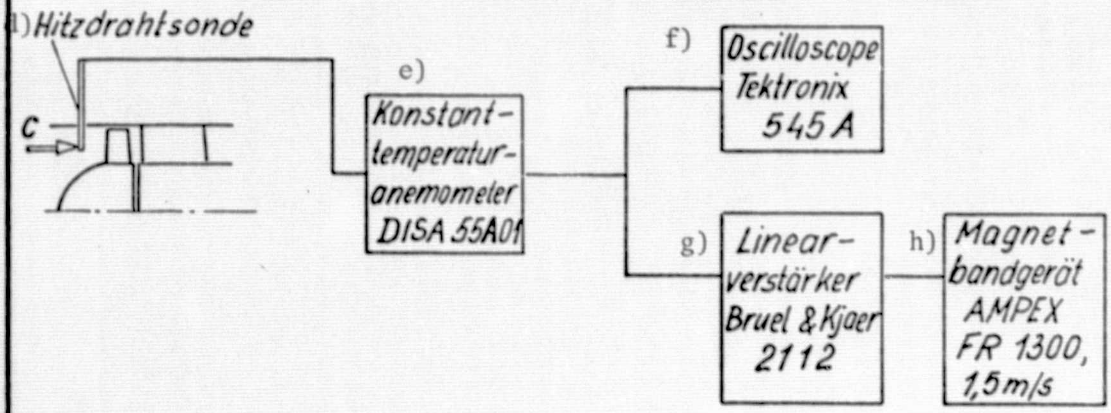

i) Frequenzanalyse des gespeicherten Hitzdrahtsignals

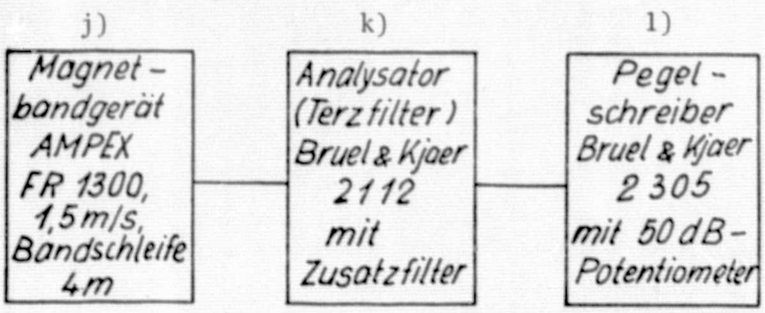

Bearbeitet: Kiock Franz	Datum: 18.9.68	Skizzenblatt Nr.:	Bericht Nr.: 68/32

Wilh. Fahrig, Braunschweig T 21300

ORIGINAL PAGE IS
OF POOR QUALITY

Deutsche Forschungsanstalt für Luft- u. Raumfahrt (DFL) Institut für Aerodynamik	Winkelcharakteristik einer Hitzdrahtsonde	Blatt Nr. 34
		Fig. 6

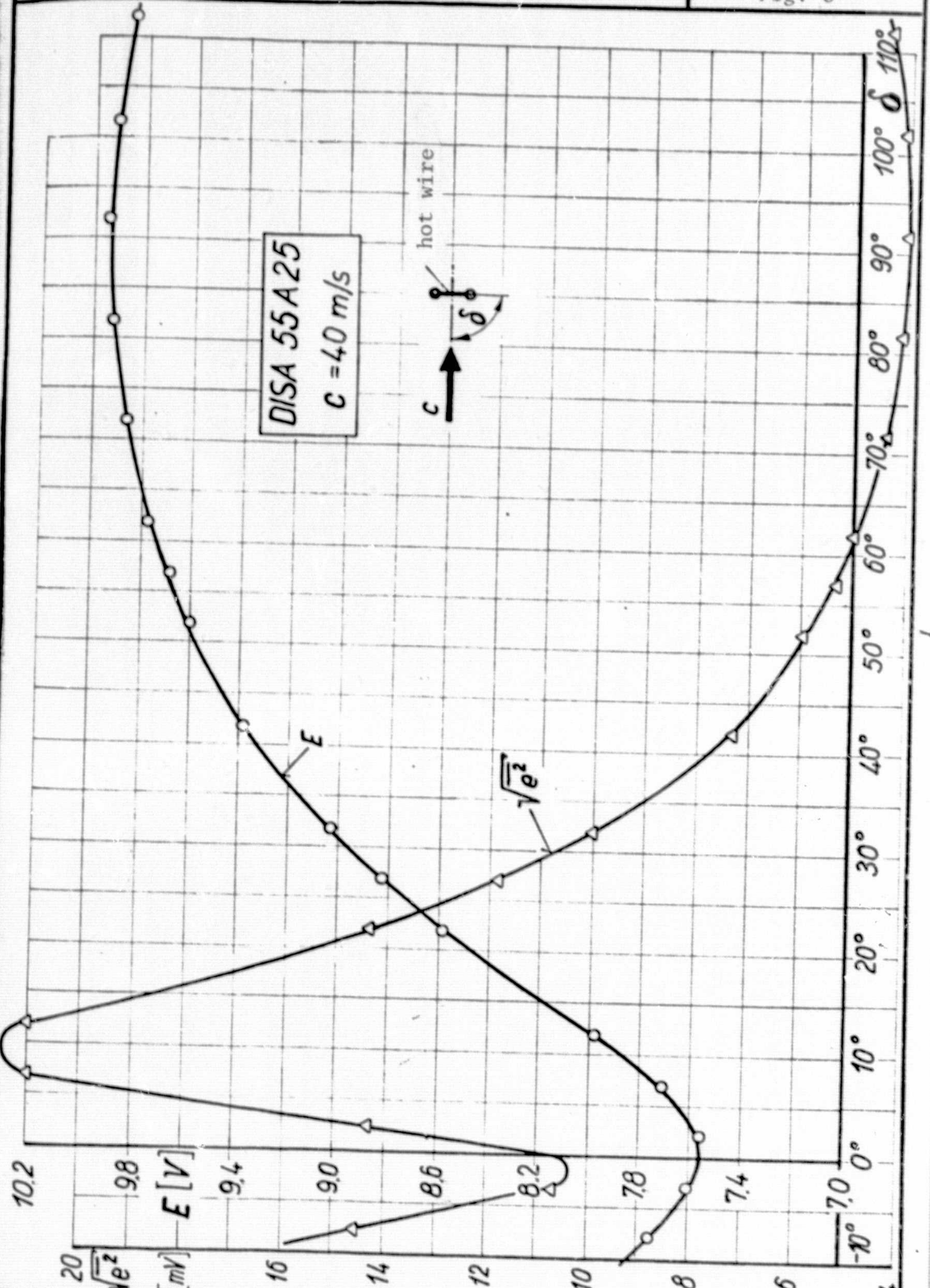

Bearbeitet: Kiock Franz	Datum: 12.9.68	Skizzenblatt Nr.:	Bericht Nr.: 68/32

Wilh. Fahrig, Braunschweig T 21300

Deutsche Forschungsanstalt für Luft- u. Raumfahrt (DFL) Institut für Aerodynamik	Geschwindigkeiten hinter einem ebenen Gitter	Blatt Nr. 35 Fig. 7

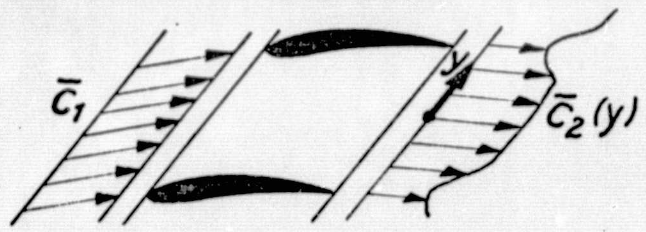

a) *Geschwindigkeit – Zeit – Diagramm an einem beliebigen Punkt y*

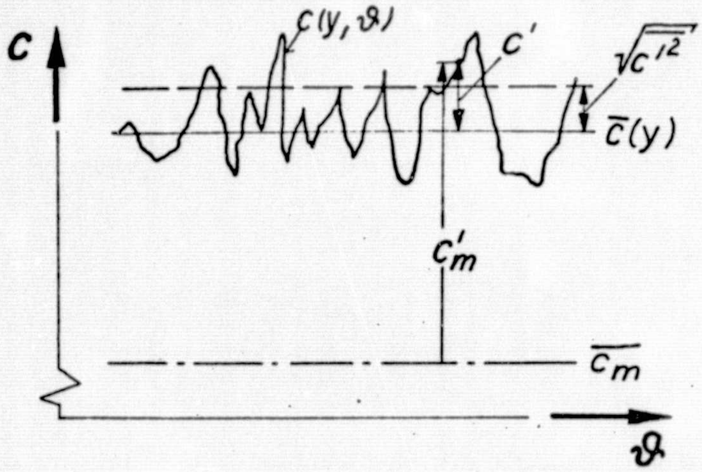

b) *Geschwindigkeit – Weg – Diagramm zu einem beliebigen Zeitpunkt ϑ*

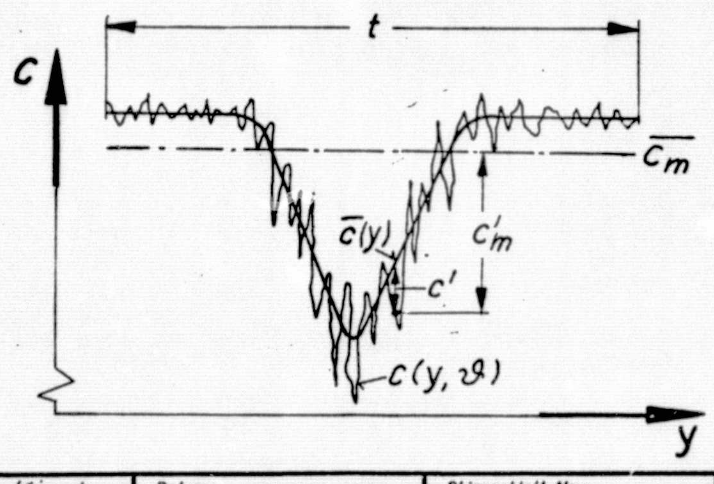

Bearbeitet: Kiock Franz	Datum: 18. 9. 68	Skizzenblatt Nr.:	Bericht Nr.: 68/32

Wilh. Fahrig, Braunschweig T 21300

Deutsche Forschungsanstalt für Luft- u. Raumfahrt (DFL) Institut für Aerodynamik	Wirkungsweise des idealen und des realen Filters	Blatt Nr. 36
		Fig. 8

a) *idealer Filter: („Kastenfilter")*
100 % Energie

b) *realer Filter:*
50 % Energie

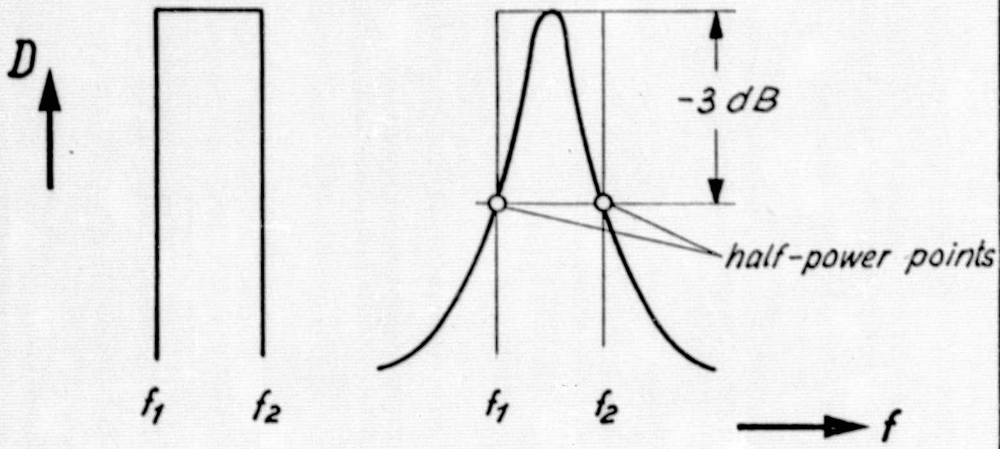

c) *Gegenseitige Beeinflussung der Filter benachbarter Frequenzbänder*

ideal Filter *real Filter*

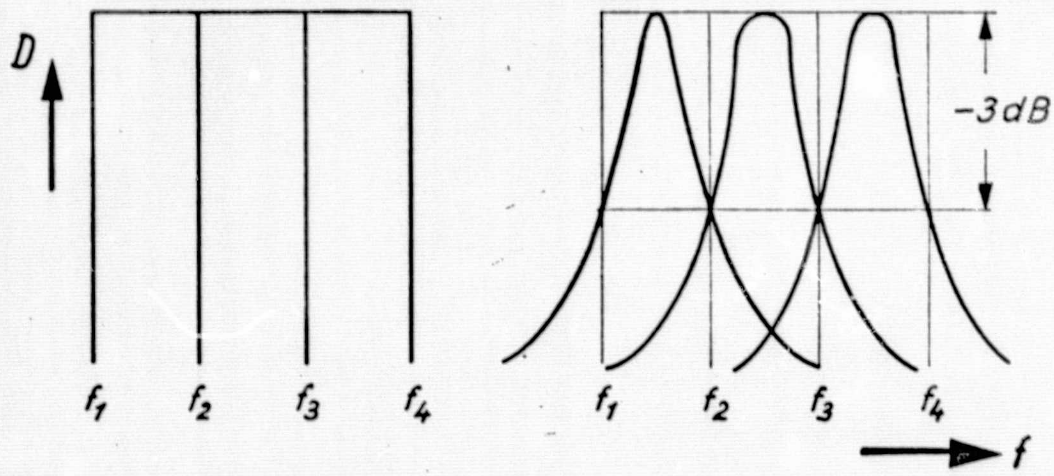

Bearbeitet: Klock Franz	Datum: 17. 9. 68	Skizzenblatt Nr.:	Bericht Nr.: 68/32

Wilh. Fahrig, Braunschweig T 21500

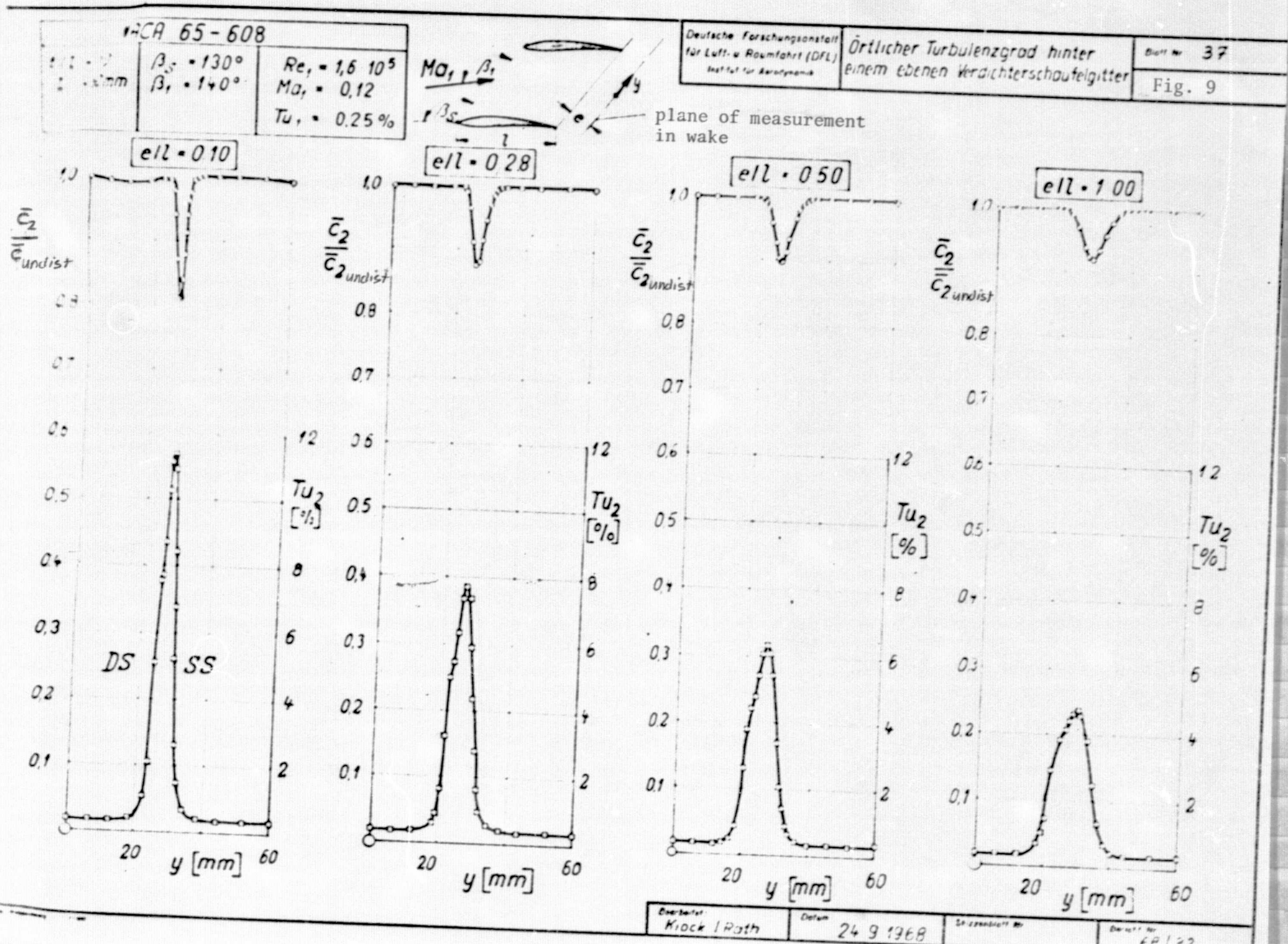

NACA 65 - 608
β_S = 130°
β_1 = 140°
Re_1 = 1,6 10^5
Ma_1 = 0,12
Tu_1 = 0,25 %
Ma_1, β_1
β_S
plane of measurement in wake
Deutsche Forschungsanstalt für Luft- u. Raumfahrt (DFL)
Institut für Aerodynamik
Örtlicher Turbulenzgrad hinter einem ebenen Verdichterschaufelgitter
37
Fig. 9
e/l = 0.10
e/l = 0.28
e/l = 0.50
e/l = 1.00
$\bar{c}_2 / \bar{c}_{2\,undist}$
Tu_2 [%]
DS
SS
y [mm]
Kiock / Rath
24.9.1968
68/32

Deutsche Forschungsanstalt für Luft- u. Raumfahrt (DFL) Institut für Aerodynamik	Örtliche Schwankungsgeschwindigkeit hinter einem ebenen Verdichterschaufelgitter	Blatt Nr. 38 / Fig. 10

NACA 65-608		
$t/l = 1{,}0$ $l = 60\,mm$	$\beta_b = 130°$ $\beta_1 = 140°$	$Re_1 = 1{,}6 \cdot 10^5$ $Ma_1 = 0{,}12$ $Tu_1 = 0{,}25\,\%$

$$\sqrt{\overline{c_2'^2}} = \frac{\sqrt{\overline{e^2}}}{\frac{dE}{d\bar{c}}}$$

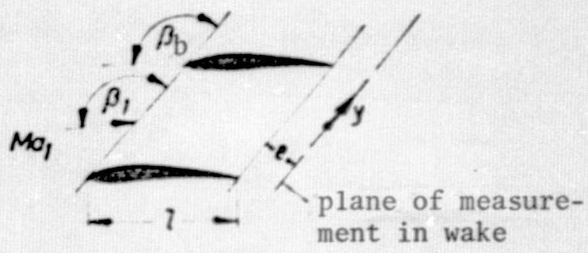

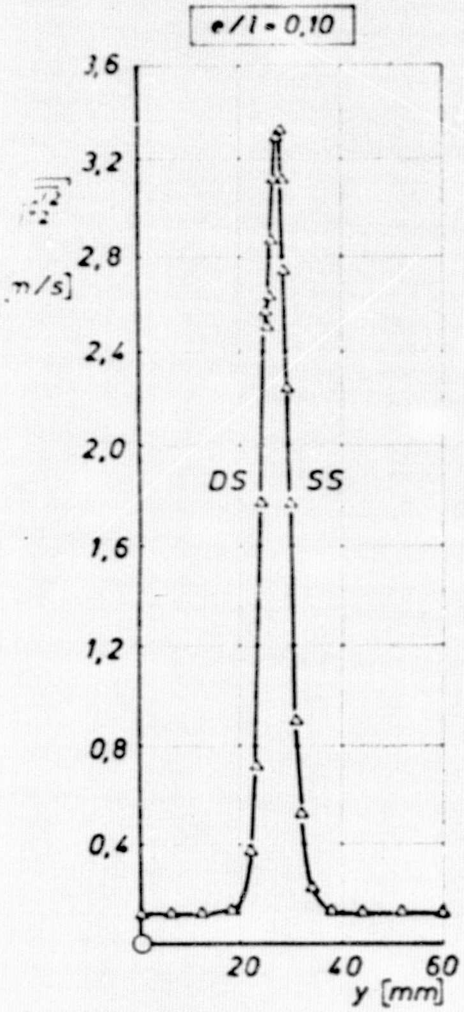

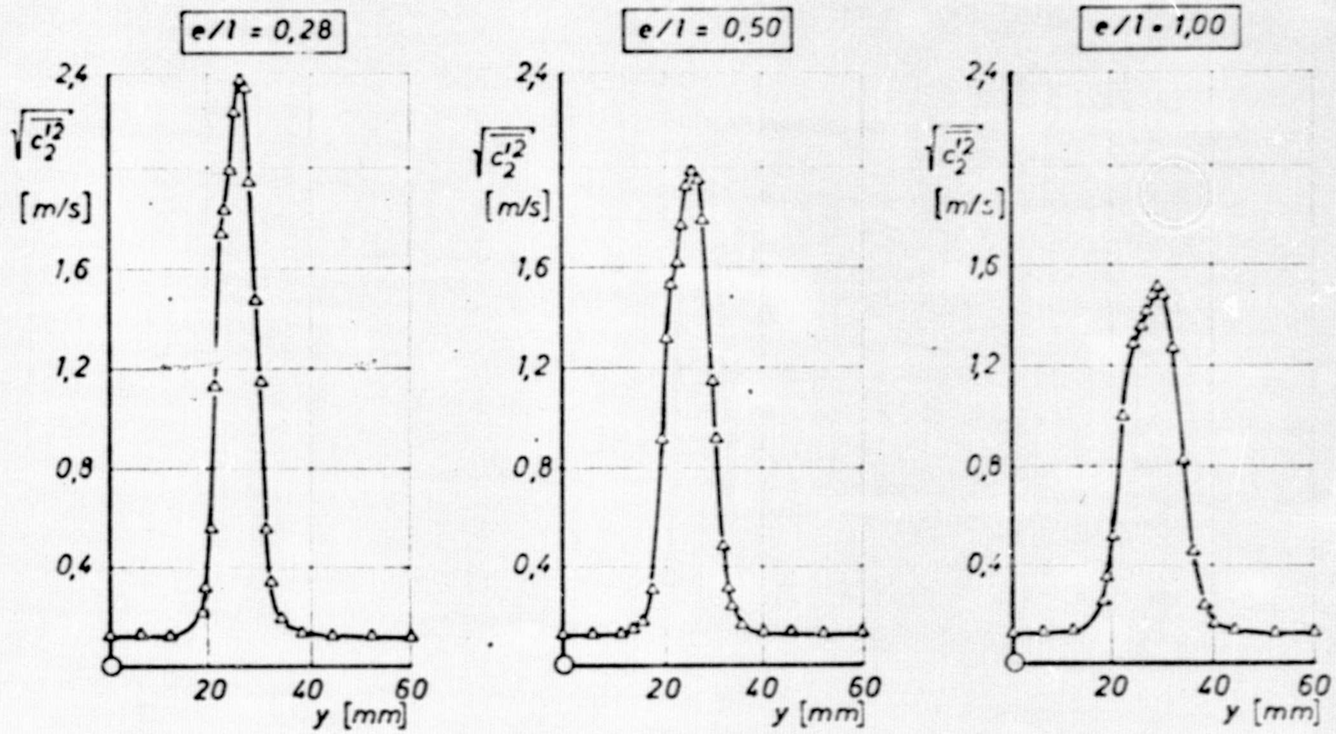

Bearbeiter: Klock Donner	Datum: 12.8.68	Skizzenblatt Nr.:	Bericht Nr. 68/32

Deutsche Forschungsanstalt für Luft- u. Raumfahrt (DFL) Institut für Aerodynamik	Einfluß der Entfernung auf den nach Gleichung (13) ermittelten Turbulenzgrad	Blatt Nr. 39 Fig. 11

NACA 65-608		
$t/l = 1{,}0$ $l = 60\,mm$	$\beta_b = 130°$ $\beta_1 = 140°$	$Re_1 = 1{,}6 \cdot 10^5$ $Ma_1 = 0{,}12$ $Tu_1 = 0{,}25\,\%$

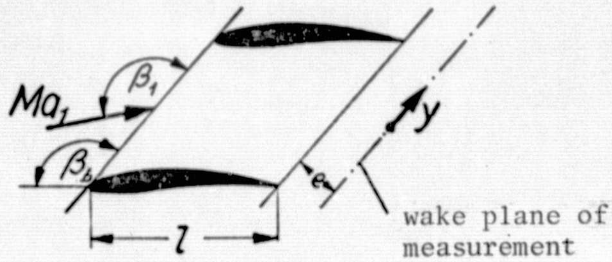

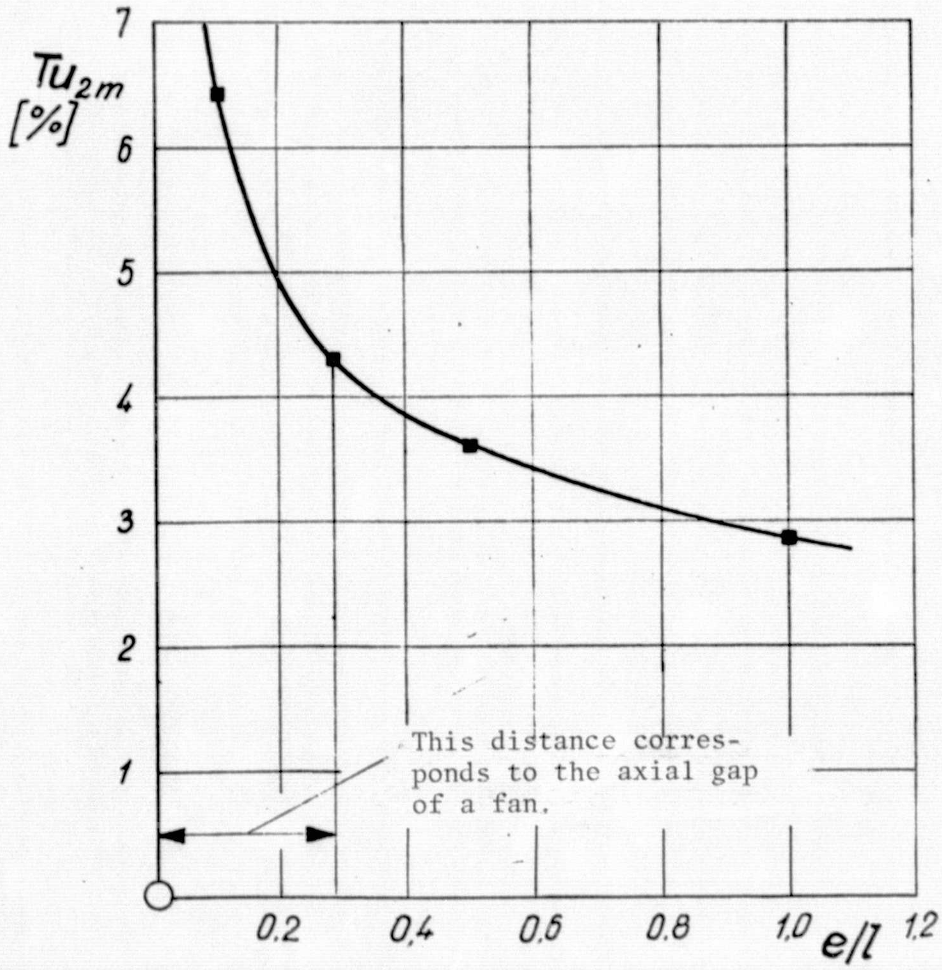

Bearbeitet: Kiock Franz	Datum: 19.9.68	Skizzenblatt Nr.:	Bericht Nr.: 68/32

Deutsche Forschungsanstalt für Luft- u. Raumfahrt (DFL) Institut für Aerodynamik	Rückwirkung der Laufschaufeln auf die Zuströmung	Blatt Nr. 40
		Fig. 12

a) Lüfter I, II und III angetrieben

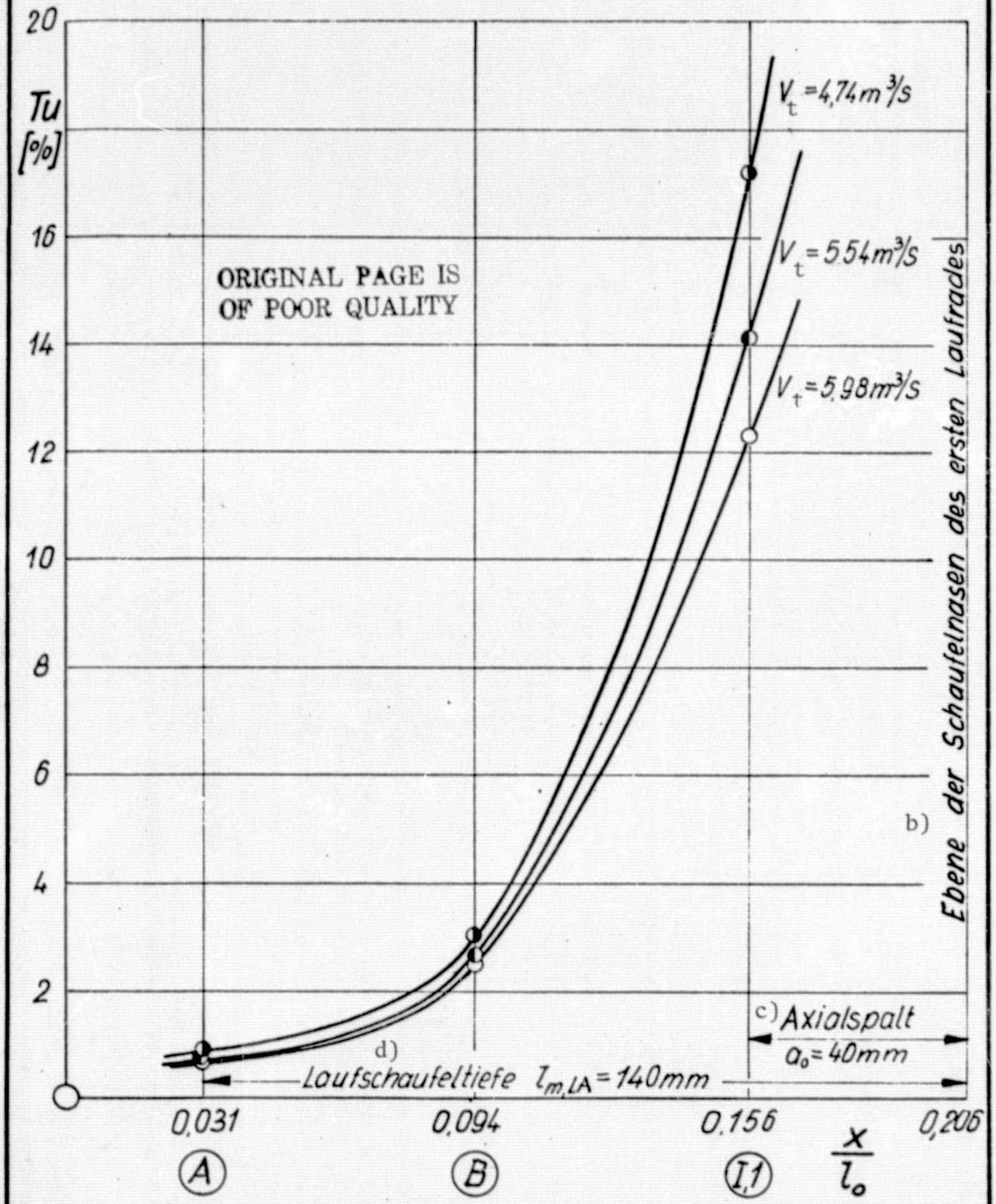

Bearbeitet: Kiock Franz	Datum: 20.9.68	Skizzenblatt Nr.:	Bericht Nr.: 68/32

Wilh. Fehrig, Braunschweig T 21300

Deutsche Forschungsanstalt für Luft- u. Raumfahrt (DFL) Institut für Aerodynamik	Turbulenzgrad entlang der Kanalachse bei drei angetriebenen Lüftern	Blatt Nr. 41
		Fig. 13

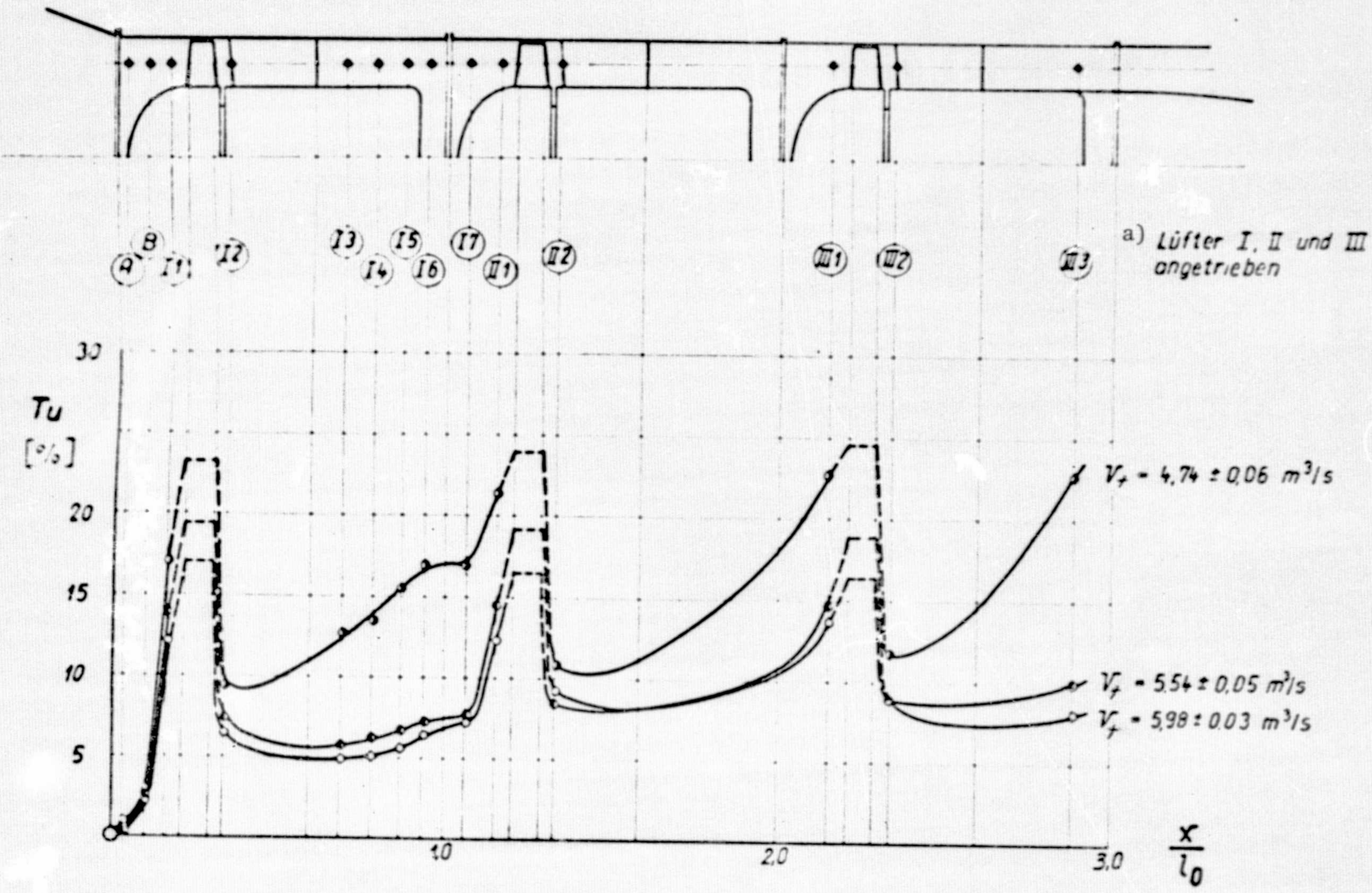

Bearbeitet:	Datum:	Skizzenblatt Nr.:	Bericht Nr.
Krock / Roth	25.9.1968		68/32

Deutsche Forschungsanstalt für Luft- u. Raumfahrt (DFL) Institut für Aerodynamik	Turbulenzgrad entlang der Kanalachse bei zwei angetriebenen Luftern	Blatt Nr. 42
		Fig. 14

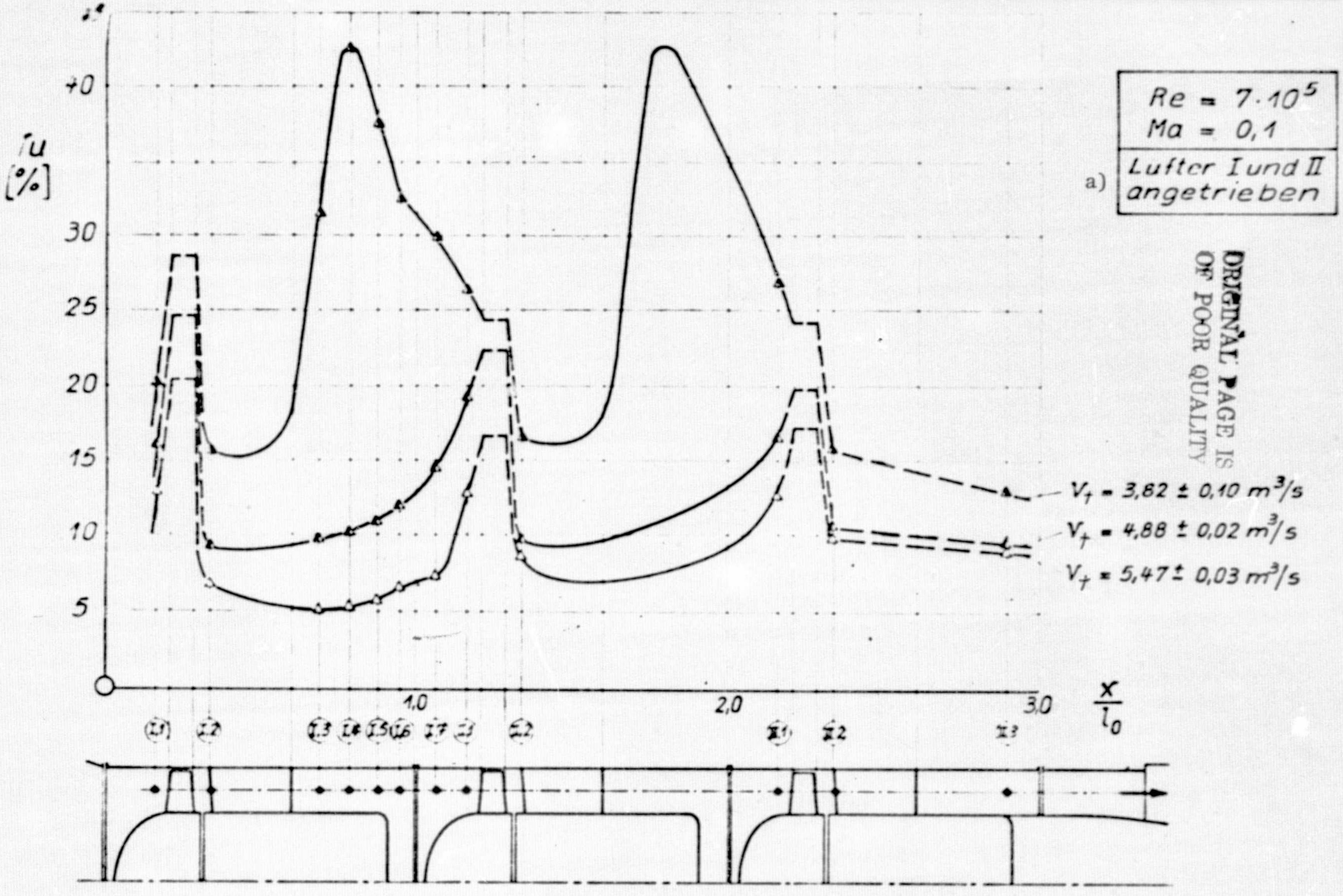

Bearbeitet: Kiock	Datum: 25.9.68	Skizzenblatt Nr.:	Bericht Nr. 68/32

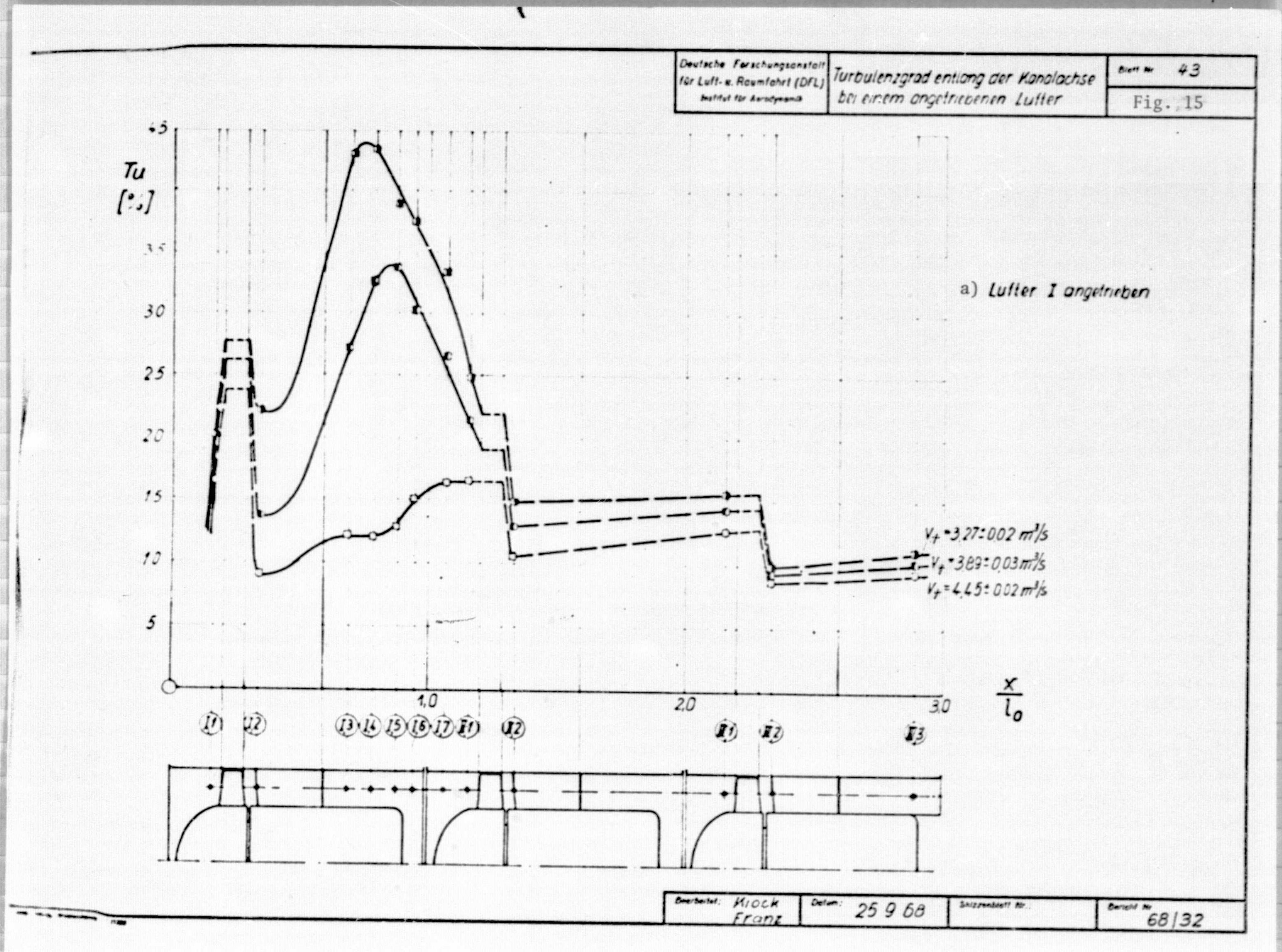

Deutsche Forschungsanstalt für Luft- u. Raumfahrt (DFL)
Institut für Aerodynamik
Turbulenzgrad entlang der Kanalachse bei einem angetriebenen Lüfter
Blatt Nr. 43
Fig. 15
Tu [%]
a) Lüfter I angetrieben
$V_t = 3{,}27 \pm 0{,}02\ m^3/s$
$V_t = 3{,}89 \pm 0{,}03\ m^3/s$
$V_t = 4{,}45 \pm 0{,}02\ m^3/s$
$\frac{x}{l_0}$
1,0
2,0
3,0
Bearbeitet: Klock Franz
Datum: 25 9 68
Skizzenblatt Nr.:
Bericht Nr. 68/32

Deutsche Forschungsanstalt für Luft- u. Raumfahrt (DFL) Institut für Aerodynamik	Verlauf des Turbulenzgrades über der Kanalhöhe vor dem ersten Laufrad	Blatt Nr. 44 Fig. 16

a) *Meßstelle I,1*

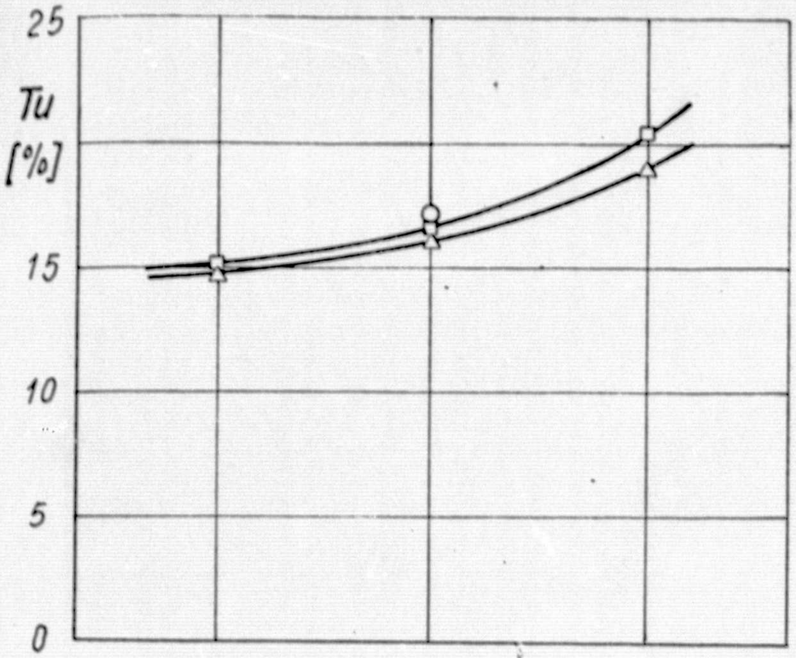

$V_t \approx const.$		
	b) angetriebene	
Symbol	Lüfter	V_t [m³/s]
□	1	4.47
△	2	4.90
○	3	4.82

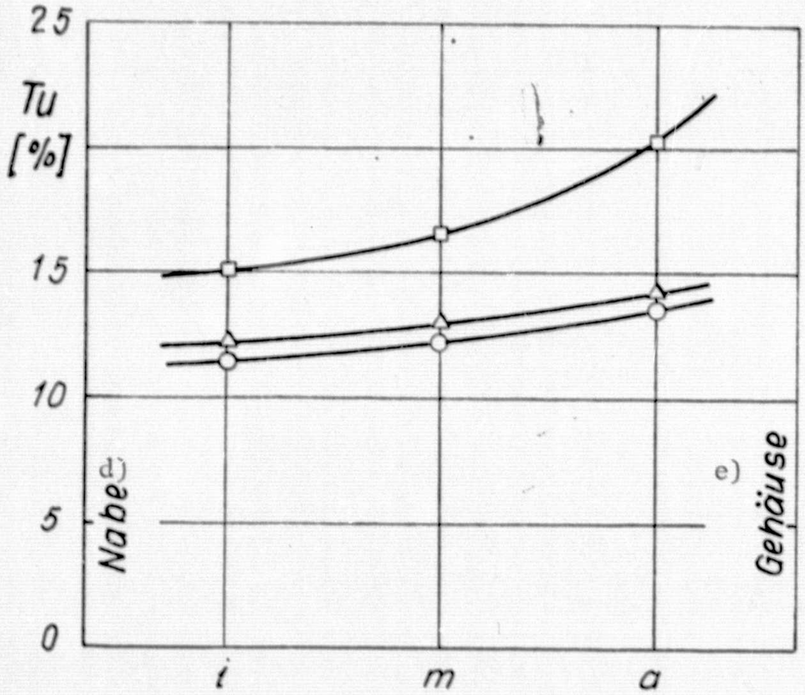

c) ungedrosselt		
	b) angetriebene	
Symbol	Lüfter	V_t [m³/s]
□	1	4.47
△	2	5.52
○	3	6.02

Bearbeitet:	Datum:	Skizzenblatt Nr.:	Bericht Nr.:
Kiock Franz	20.9.68		68/32

Wilh. Fehrig, Braunschweig T 21300

Deutsche Forschungsanstalt für Luft- u. Raumfahrt (DFL) Institut für Aerodynamik	Verlauf des Turbulenzgrades über der Kanalhöhe hinter dem ersten Laufrad	Blatt Nr. 45
		Fig. 17

a) Meßstelle I,2

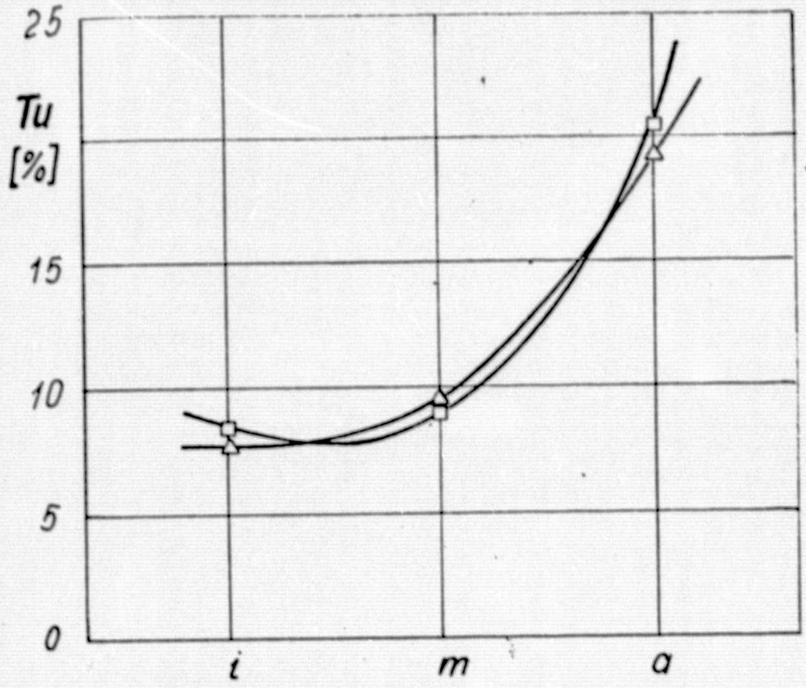

$V_t \approx$ const.		
b) angetriebene		
Symbol	Lüfter	V_t [m³/s]
□	1	4.47
△	2	4.90
○	3	4.79

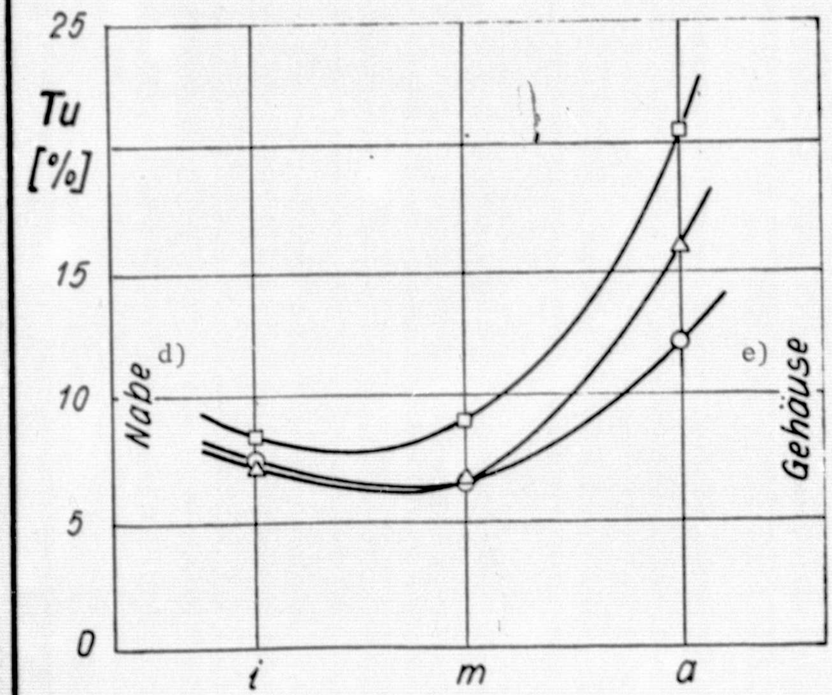

c) ungedrosselt		
b) angetriebene		
Symbol	Lüfter	V_t [m³/s]
□	1	4.47
△	2	5.52
○	3	6.02

Bearbeitet: Kiock Franz	Datum: 23.9.68	Skizzenblatt Nr.:	Bericht Nr.: 68/32

Wilh. Fahrig, Braunschweig T 21300

Deutsche Forschungsanstalt für Luft- u. Raumfahrt (DFL) Institut für Aerodynamik	Verlauf des Turbulenzgrades über der Kanalhöhe hinter der ersten Stufe	Blatt Nr. 46
		Fig. 18

a) Meßstelle I, 5

ORIGINAL PAGE IS OF POOR QUALITY

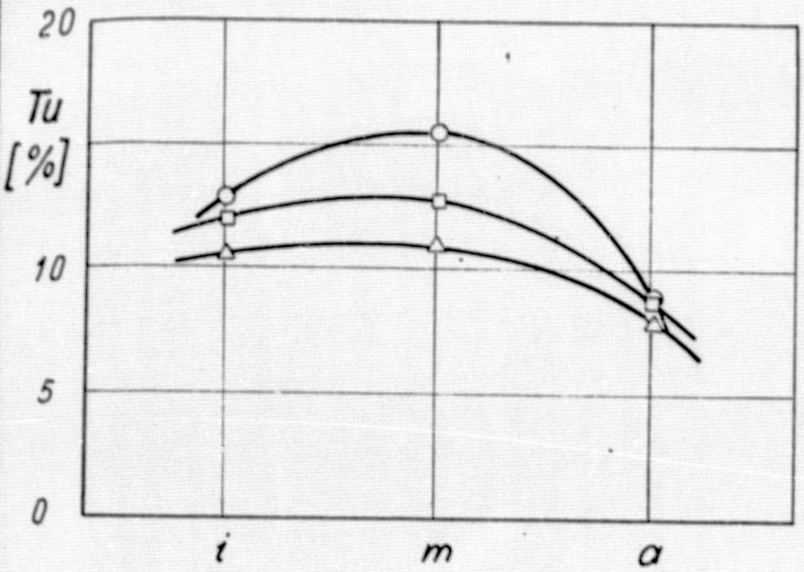

$V_+ \approx const.$		
b) angetriebene		
Symbol	Lüfter	$V_+ [m^3/s]$
□	1	4.43
△	2	4.90
○	3	4.72

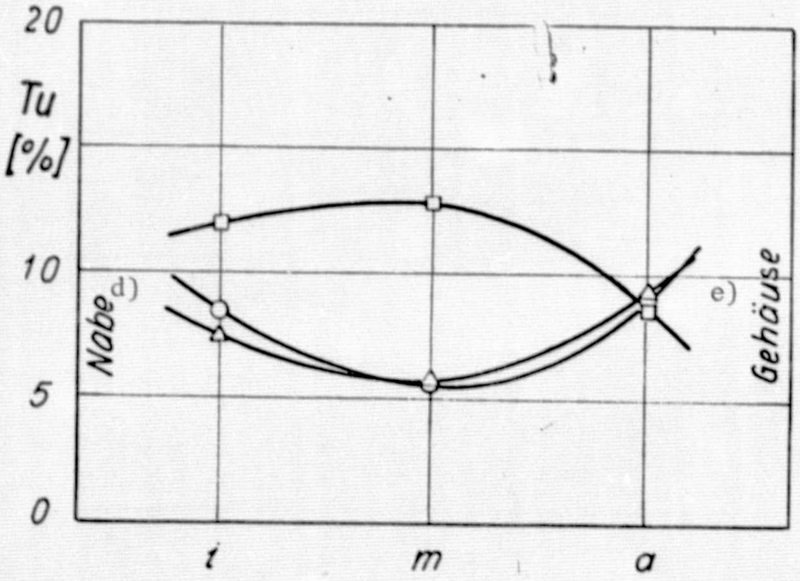

c) ungedrosselt		
b) angetriebene		
Symbol	Lüfter	$V_+ [m^3/s]$
□	1	4.43
△	2	5.46
○	3	5.98

Bearbeitet: Klock Franz	Datum: 23.9.68	Skizzenblatt Nr.:	Bericht Nr.: 68/32

Wilh. Fahrig, Braunschweig T 21300

Deutsche Forschungsanstalt für Luft- u. Raumfahrt (DFL) Institut für Aerodynamik	Verlauf des Turbulenzgrades in der Leitradradeintrittsebene des ersten Lüfters	Blatt Nr. 47
		Fig. 19

a) *Meßstelle I, 2*

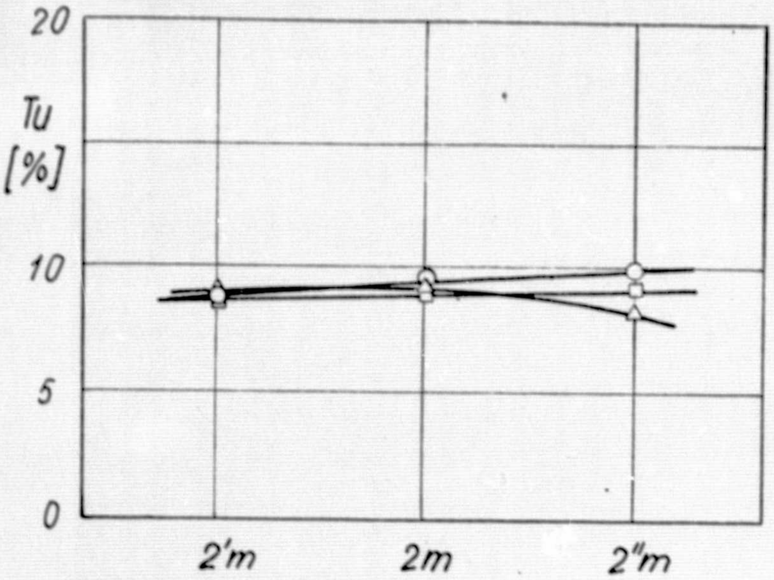

$V_+ \approx$ const.		
b) angetriebene		
Symbol	Lüfter	V_+ [m³/s]
□	1	4.46
△	2	4.88
○	3	4.77

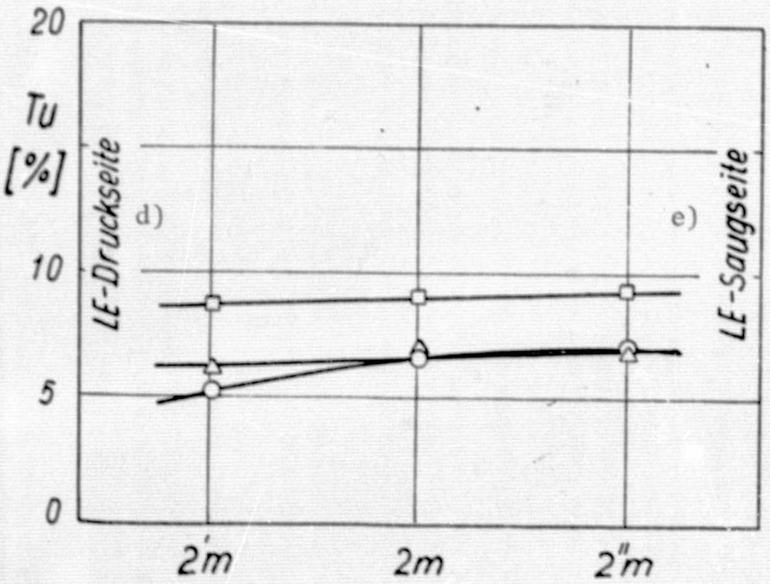

c) ungedrosselt		
b) angetriebene		
Symbol	Lüfter	V_+ [m³/s]
□	1	4.46
△	2	5.48
○	3	5.99

Bearbeitet: Kiock Franz	Datum: 24.9.68	Skizzenblatt Nr.:	Bericht Nr.: 68/32

Deutsche Forschungsanstalt für Luft- u. Raumfahrt (DFL) Institut für Aerodynamik	Einfluß des Durchsatzes auf den Turbulenzgrad im ersten Lüfter	Blatt Nr. 48
		Fig. 20

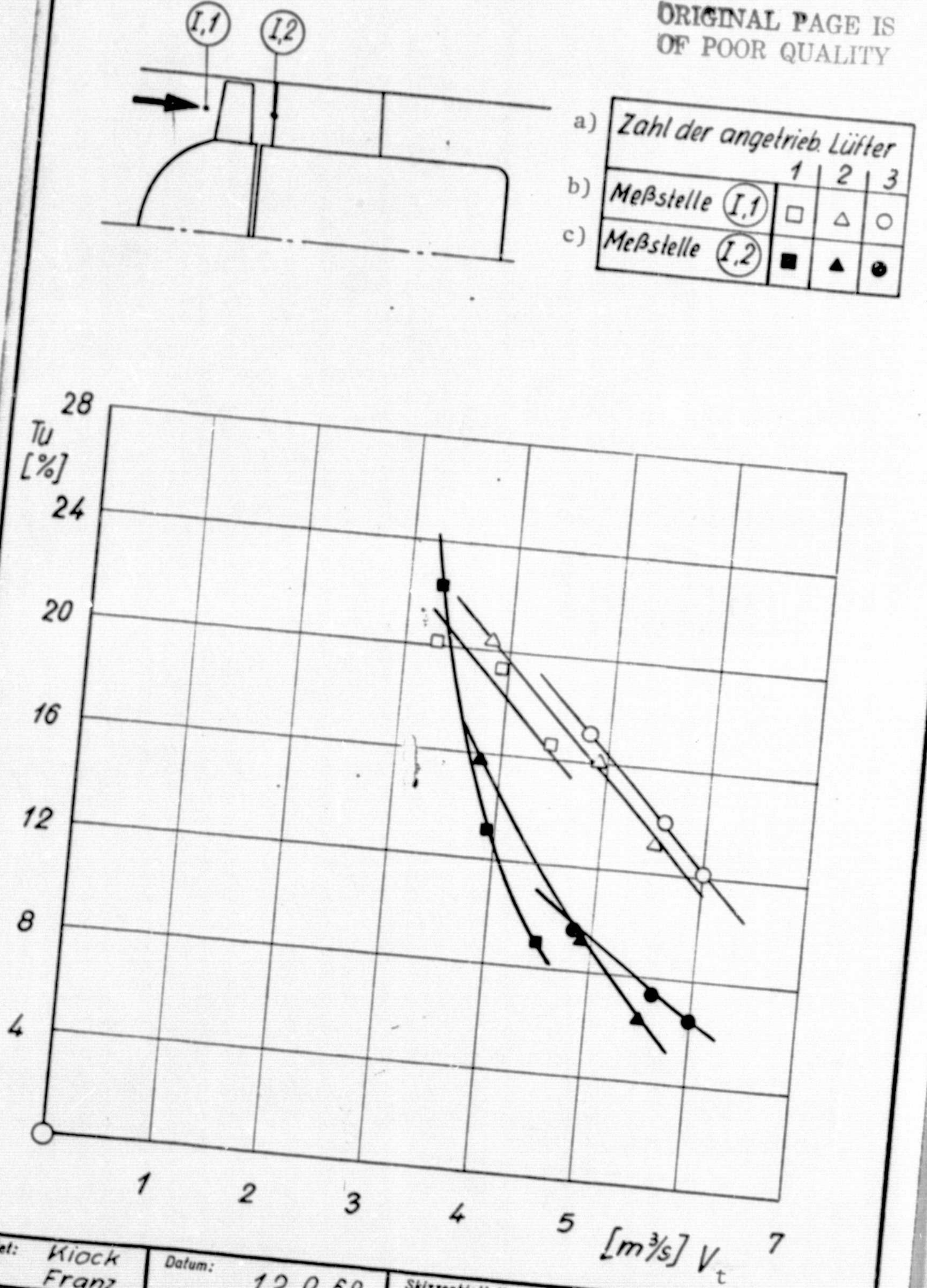

Bearbeitet: Klock Franz	Datum: 12.9.68	Skizzenblatt Nr.:	Bericht Nr.: 68/32

Wilh. Fahrig, Braunschweig T 21300

Deutsche Forschungsanstalt für Luft- u. Raumfahrt (DFL) Institut für Aerodynamik	Einfluß des Durchsatzes auf den Turbulenzgrad im zweiten Lüfter	Blatt Nr. 49 Fig. 21

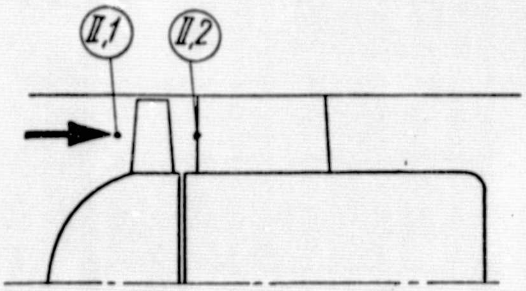

	Zahl der angetrieb. Lüfter		
	1	2	3
a)			
b) Meßstelle II,1	□	△	○
c) Meßstelle II,2	■	▲	●

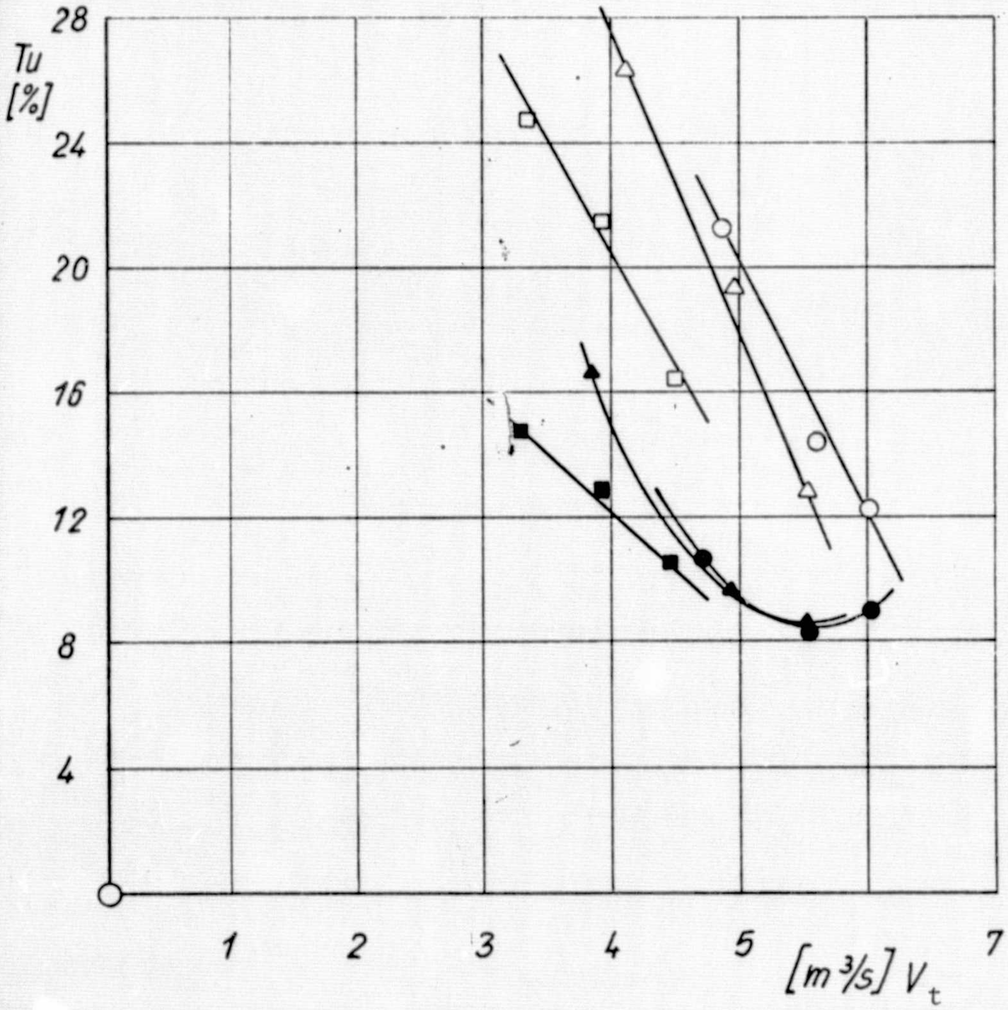

Bearbeitet: Klock Franz	Datum: 12.9.68	Skizzenblatt Nr.:	Bericht Nr.: 68/32

Wilh. Fahrig, Braunschweig T 21300

Deutsche Forschungsanstalt für Luft- u. Raumfahrt (DFL) Institut für Aerodynamik	Einfluß des Durchsatzes auf den Turbulenzgrad im dritten Lüfter	Blatt Nr. 50
		Fig. 22

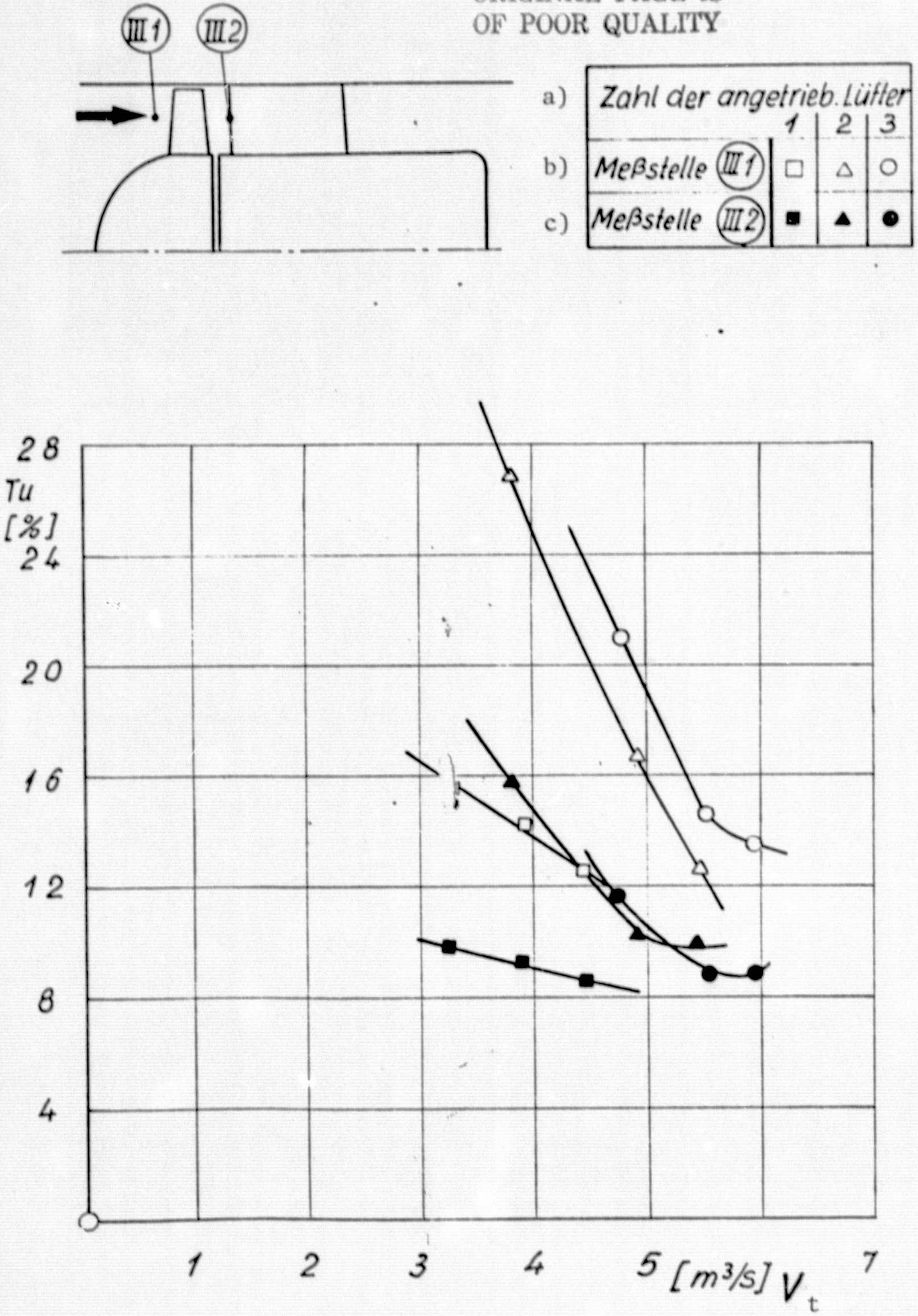

Bearbeitet: Klock Franz	Datum: 9.9.68	Skizzenblatt Nr.:	Bericht Nr.: 68/32

Wdh. Fahrig, Braunschweig T 21300

Deutsche Forschungsanstalt für Luft- u. Raumfahrt (DFL) Institut für Aerodynamik	Frequenzspektren am ersten Lüfter bei unterschiedlichem Durchsatz	Blatt Nr. 51
		Fig. 23

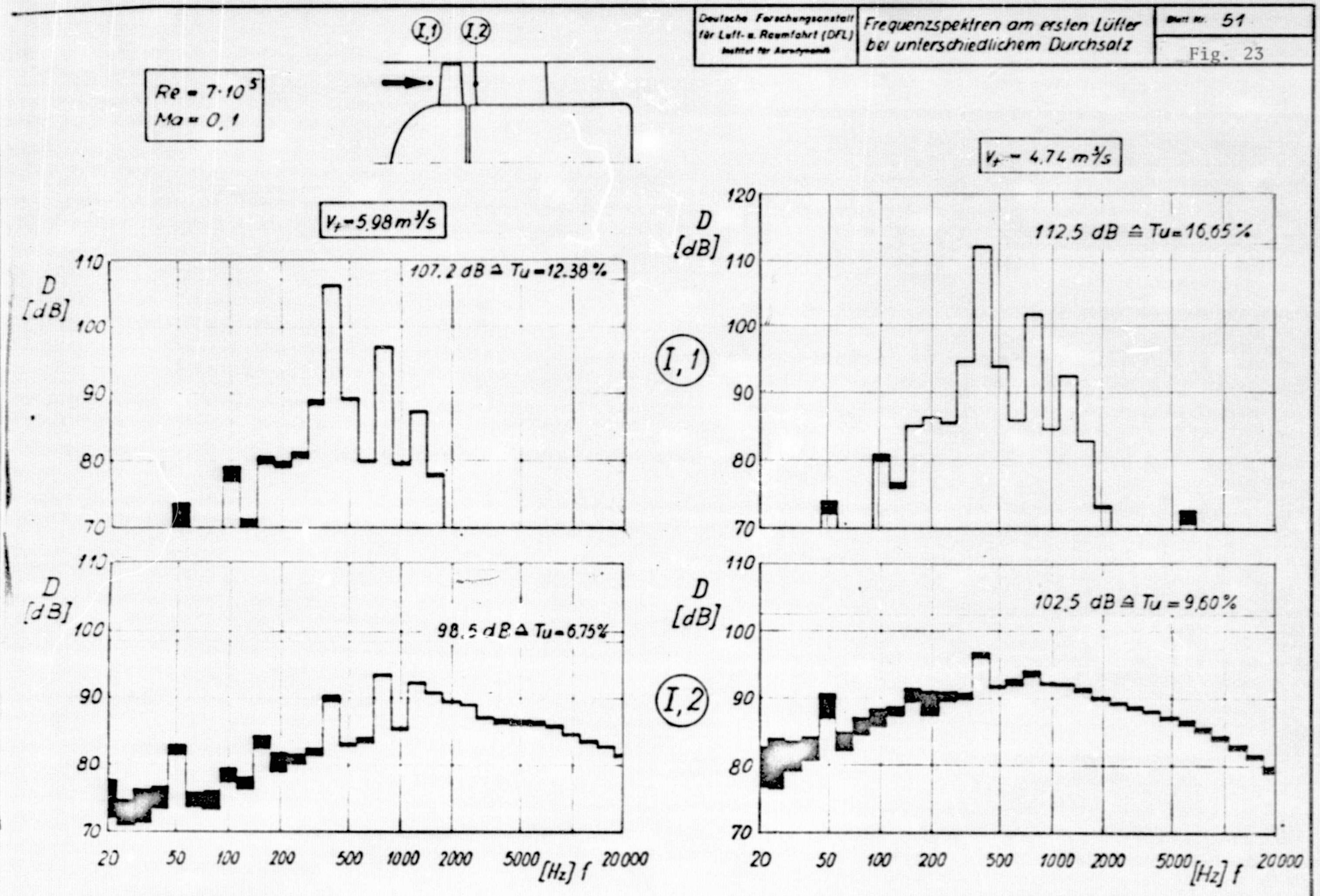

Bearbeitet: Klock Franz	Datum: 11 9 68	Skizzenblatt Nr.:	Bericht Nr. 68/32

Deutsche Forschungsanstalt für Luft- u. Raumfahrt (DFL) Institut für Aerodynamik	Frequenzspektren am zweiten Lüfter	Blatt Nr. 52 / Fig. 24

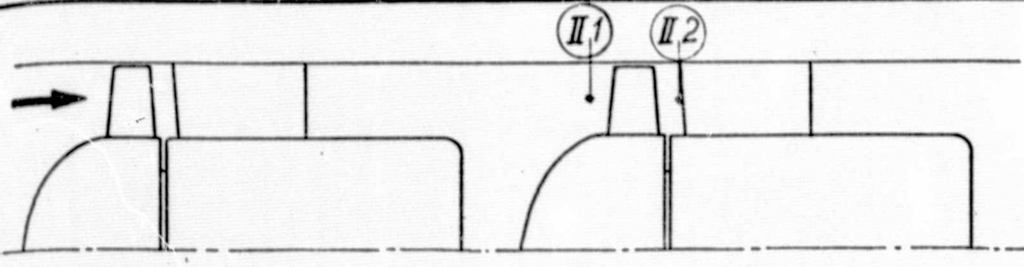

$Re = 7 \cdot 10^5$
$Ma = 0.1$
$V_t = 5{,}98\ m^3/s$

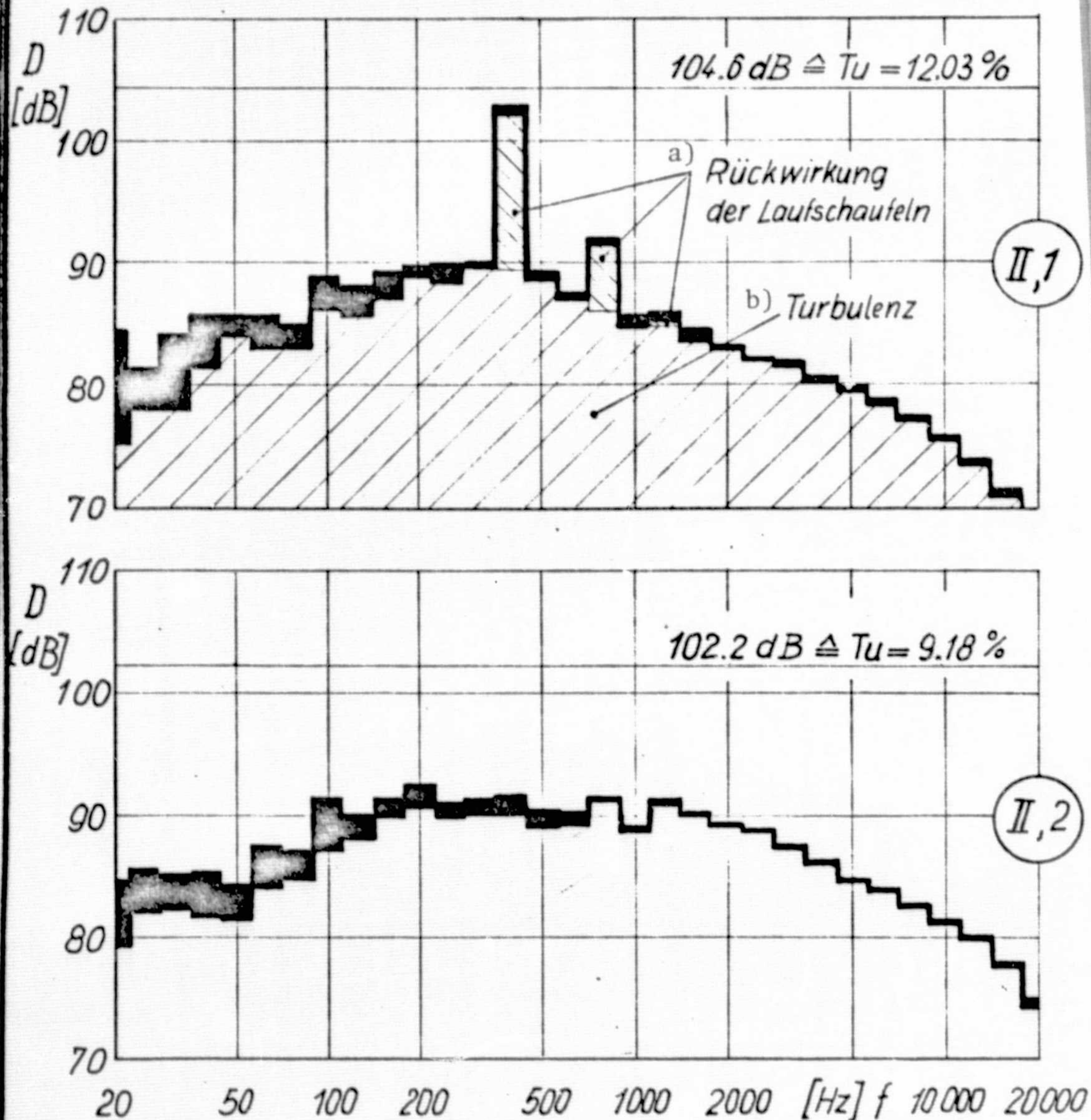

Bearbeitet: Kiock Franz	Datum: 10. 9. 68	Skizzenblatt Nr.:	Bericht Nr.: 68/32

Wilh. Fahrig, Braunschweig T 21300

Deutsche Forschungsanstalt für Luft- u. Raumfahrt (DFL) Institut für Aerodynamik	Gemessener und korrigierter Turbulenzgrad entlang d. Kanalachse	Blatt Nr. 53 Fig. 25

a) Lüfter I, II und III angetrieben ; $V_t = 5.98\ m^3/s$

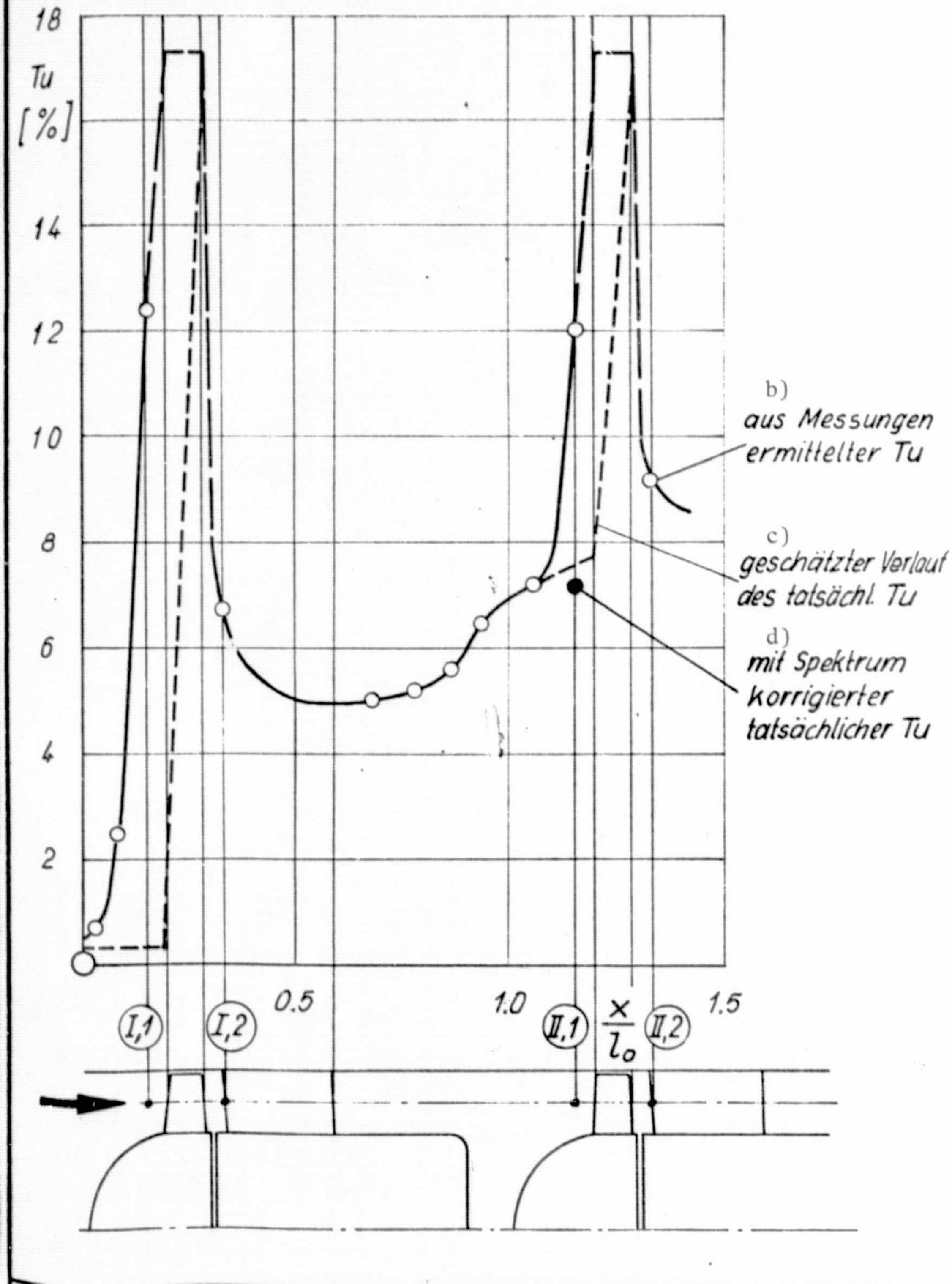

Bearbeitet: Kiock Franz	Datum: 9. 9. 68	Skizzenblatt Nr.:	Bericht Nr.: 68/32

Wilh. Fahrig, Braunschweig T 21300